

Integration of Microwave and Millimeter Wave Bandpass Filters with Antennas

by
Hanyue Xu

A Thesis Submitted in Partial Fulfillment
of the Requirements for the Degree of
Master of Applied Science

In

Electrical and Computer Engineering
The Faculty of Engineering and Applied Science

University of Ontario Institute of Technology

July 2016

© Copyright by Hanyue Xu, 2016

TABLE OF CONTENTS

TABLE OF CONTENTS.....	ii
LIST OF FIGURES	iv
LIST OF ABBREVIATIONS.....	ix
ABSTRACT.....	x
ACKNOWLEDGEMENTS	xii
CHAPTER 1: Introduction	1
1.1 Overview.....	1
1.2 Motivation.....	2
1.3 Contributions.....	4
1.4 Thesis Outline	5
CHAPTER 2: Literature Review	7
2.1 Filter and Antenna Integration	7
2.2 Dielectric Resonator Antenna (DRA).....	11
2.3 Substrate Integrated Waveguide	12
CHAPTER 3: Integration of DRA and SIW Filter	15
3.1 Design of SIW Filter.....	16
3.2 Design of Dielectric Resonator Antenna	24
3.3 Filter Antenna Integration.....	28
3.4 Tuning of the Structure	34
3.5 Coaxial to SIW Transition	39
3.6 Integration of Filter with DRA Array	47
3.7 Integration of Filter with Parasitic DRA.....	56

3.8 Measurement Results	59
3.9 Summary	66
CHAPTER 4: Integration of Microstrip Bandpass Filter with Inset-Fed Patch Antenna.	68
4.1 Design of the Filter	69
4.2 Design of the Inset-Fed Microstrip Patch Antenna.....	72
4.3 The Integration of the Inset-Fed Antenna and Filter	76
4.4 Design Example and Simulation Results	80
4.5 Summary	82
CHAPTER 5: Conclusion and Furture Work	83
BIBLIOGRAPHY	86

LIST OF FIGURES

Fig. 1. 1. The general concept of filter and antenna integration.	3
Fig. 2. 1. Equivalent circuit model of bandpass filter with impedance inverter.	9
Fig. 2. 2. Schematic of rectangular DRA fed by rectangular waveguide.	12
Fig. 2. 3. Model of SIW, with two rows of via holes.....	13
Fig. 3. 1. 3D model of SIW four-pole bandpass filter.	18
Fig. 3. 2. Top view of the four pole SIW filter.	19
Fig. 3. 3. The parameters of SIW.....	20
Fig. 3. 4. The S parameters of the four-pole filter.	20
Fig. 3. 5. The generation of equivalent circuit model of SIW filter.	22
Fig. 3. 6. The schematic of equivalent circuit model in ADS, showing the first two cavities.	22
Fig. 3. 7. S-parameters of equivalent circuit model in ADS and the SIW filter design in HFSS.....	24
Fig. 3. 8. DRA dimensions.....	25
Fig. 3. 9. The top view and side view of SIW-based DRA.....	26
Fig. 3. 10. The EM simulation results of SIW-based DRA structure	27
Fig. 3. 11. 3-D model of SIW filter and DRA integration.	29
Fig. 3. 12. Top view of filter antenna integration.	29
Fig. 3. 13. Flow chart for filter antenna integration.....	30
Fig. 3. 14. Configuration of DRA and its equivalent circuit model.....	31

Fig. 3. 15. (a) Phase of S_{11} and (b) the normalized input impedance of design in HFSS and equivalent RLC circuit.....	32
Fig. 3. 16. The design curve of Q_{ext} vs. X_{sc} and L_s	34
Fig. 3. 17. The equivalent circuit for DRA.....	35
Fig. 3. 18. Equivalent circuit model of SIW-fed DRA in ADS.....	36
Fig. 3. 19. The equivalent circuit models for (a) SIW filter and (b) filter antenna integration.	37
Fig. 3. 20. Simulated $ S_{11} $ of the filter antenna integration before optimization.	37
Fig. 3. 21. Simulated $ S_{11} $ of the filter antenna integration after fine tuning.	38
Fig. 3. 22. Equivalent circuit model for bandpass filter and filter antenna integration.	39
Fig. 3. 23. 3-D model of back-to-back coax-to-SIW transitions.	40
Fig. 3. 24. Top view of the back-to-back coax-to-SIW transitions.....	41
Fig. 3. 25. The impact of coax position d_{sc} variation on $ S_{11} $ (dB), $d_x=2.18$ mm, and $d_y=3.35$ mm.	42
Fig. 3. 26. The impact of tuning screws x-position d_x variation on $ S_{11} $ (dB).....	43
Fig. 3. 27. The impact of tuning screws y-position d_y variation on $ S_{11} $ (dB).....	43
Fig. 3. 28. The simulated $ S_{11} $ of back-to-back transitions compared with $ S_{11} $ of filter and antenna integration.....	44
Fig. 3. 29. 3-D model of SIW filter and DRA integration with coax-to-SIW transition. .	45
Fig. 3. 30. Top view of SIW filter DRA integration with coax-to-SIW transition.	45
Fig. 3. 31. $ S_{11} $ of DRA and filter integration with coax-to-SIW transition.	46
Fig. 3. 32. Radiation pattern of DRA and filter integration.....	46
Fig. 3. 33. The schematic of 6-element DRA array.....	47

Fig. 3. 34. Design of two-element DRA array.....	48
Fig. 3. 35. Phase of S_{11} of DRA array.....	49
Fig. 3. 36. Normalized input impedance of DRA array in HFSS and its equivalent circuit model in ADS.	49
Fig. 3. 37. The design curve of Q_{ext} vs. X_{sc}	50
Fig. 3. 38. 3-D model of SIW filter and two-element DRA array integration.....	51
Fig. 3. 39. Top view and side view of SIW filter and two-element DRA array integration	51
Fig. 3. 40. The match of fine model from HFSS and coarse model in ADS.	52
Fig. 3. 41. Radiation pattern of filter with DRA array integration.	53
Fig. 3. 42. 3-D model of SIW filter and 6-element DRA array integration.....	54
Fig. 3. 43. Top view of the model.....	54
Fig. 3. 44. (a) $ S_{11} $ of SIW filter and 6-element DRA array integration model, and (b) radiation pattern of the model.	56
Fig. 3. 45. The parasitic DRA.	57
Fig. 3. 46. SIW filter and parasitic DRA integration.	57
Fig. 3. 47. (a) $ S_{11} $ of SIW filter and parasitic DRA integration, and (b) the radiation pattern of filter and parasitic DRA integration.	58
Fig. 3. 48. Photograph of SIW-based DRA structure.	59
Fig. 3. 49. $ S_{11} $ of simulation and measurement for SIW-based DRA model.....	60
Fig. 3. 50. $ S_{11} $ of measurement and simulation with $\epsilon_r=2.87$	61
Fig. 3. 51. $ S_{11} $ of measurement and simulation results.	61
Fig. 3. 52. Photograph of SIW filter with DRA integration.	62

Fig. 3. 53. Simulation and measurement results for filter with single DRA integration. .	63
Fig. 3. 54. Tolerance analysis for filter with single DRA integration and measurement results.....	64
Fig. 3. 55. Photograph of SIW filter with parasitic DRA integration.....	64
Fig. 3. 56. Simulation and measurement results for filter with parasitic DRA integration.	65
Fig. 3.57. Tolerance analysis for filter with parasitic DRA integration and measurement results.	68
Fig. 4. 1. Three-pole hairpin bandpass filter.....	70
Fig. 4. 2. Design curve of Q_{ext} vs. distance d_1 , and the simulation model.	71
Fig. 4. 3. Design curve of coupling coefficient k_{ij} vs. distance d_2 , and the simulation model.	72
Fig. 4. 4. 3-D model of inset-fed rectangular patch antenna.....	74
Fig. 4. 5. Top view of antenna model	74
Fig. 4. 6. EM simulated $ S_{11} $ of inset-fed rectangular patch antenna.	75
Fig. 4. 7. Radiation pattern of inset-fed rectangular patch antenna.	75
Fig. 4. 8. The direct connection coupling method between the filter resonator and the antenna.	76
Fig. 4. 9. The circuit flow on the resonator when coupled to the antenna.	77
Fig. 4. 10. The proximity coupling method between the filter resonator and the antenna [66].....	78
Fig. 4. 11. Comparison of the coupling coefficients realized using proximity and direct connection coupling methods.	79

Fig. 4. 12. An example of filter antenna integration 80

Fig. 4. 13. Reflection coefficients of the bandpass filter and the filter antenna integration.
..... 81

Fig. 4. 14. Simulated radiation pattern of the patch antenna and filter antenna integration.
..... 81

LIST OF ABBREVIATIONS

ADS	Advanced Design System
DRA	Dielectric Resonator Antenna
EM	Electromagnetic
HFSS	High Frequency Structural Simulator
PE	Parameter Extraction
Q-factor	Quality-factor
RF	Radio Frequency
SIW	Substrate Integrated Waveguide
T.L.	Transmission Line

ABSTRACT

Filters and antennas are essential elements in communication and radar systems. In a conventional design, antennas and filters are designed independently and then connected together through transitions and/or connectors, which introduces loss and increases the size of the design. Filter and antenna integration can be implemented using the resonance characteristic of the antenna and the coupling between the antenna and resonator of the filter, which effectively removes the transitions between the filter and antenna and improves the overall system performance. In this thesis, two different types of filter and antenna integrations are investigated.

First, the Substrate Integrated Waveguide (SIW) filter integration with dielectric resonator antenna (DRA) in millimeter-wave frequency range is presented. SIW is used to design the bandpass filter and serves as the feeding structure for DRA. Design integration with improved radiation efficiency is achieved by replacing the last resonator of the filter with DRA. The synthesis procedure is presented in detail. Equivalent circuit models are developed to facilitate optimizations of the design. In addition, integrated designs of parasitic DRA and DRA arrays with SIW filters are developed. All designs have been simulated and fine-tuned using full wave solver. Simulation and measurement results are presented.

Second, a microstrip bandpass filter integrated with patch antenna is also studied for improvement of the range of the coupling coefficient. The coupling between the antenna and the filter is achieved by direct connection of the feed line of the patch antenna and the resonator of the filter, which increases the coupling value between the filter and the antenna. A comparative study is made to show the improvement. This method provides large range of coupling coefficient, which leads to wider achievable bandwidth.

ACKNOWLEDGEMENTS

I would like to express my appreciation to my supervisor Dr. Ying Wang for her great help. During my two years' graduate study and research in the Master's program, Dr. Ying Wang has always been helpful and patient. I have learned a lot from her. Also, I would like to thank all my colleagues and friends for their kind supports. In the end, I am grateful to my parents for their love.

Hanyue Xu

Oshawa, Ontario

July, 2016

CHAPTER 1

Introduction

1.1 Overview

The rapid development of wireless communication and radar systems demands high performance, compact, and low-cost circuits and devices. Filters and antennas are essential elements in communication systems. As a result, constraints such as low profile, compact size, high efficiency, and low price are important requirements for the design of filters and antennas.

Microwave and millimeter-wave circuits, including filters and antennas, can be realized in planar and non-planar technologies. Non-planar circuits, for example rectangular waveguides, are often used for applications requiring high-Quality (Q) factor (low loss)

and high power. However, they are usually bulky and costly. In addition, transitions to planar circuits can be complicated. Microstrip circuits, a typical type of planar circuits, are widely used in microwave applications due to their low-profile, ease of fabrication, ease of integration, and low cost. The main disadvantages are that the loss can be high and power handling capability is low. Substrate Integrated Waveguide (SIW) technology has recently attracted a lot of attention, which implements rectangular waveguide within the substrate of planar circuits using metallized vias inside the dielectric substrate [1], [2]. It offers advantages, such as improved loss performance comparing to conventional planar circuits, compactness, and ease of integration with planar circuits. It can be easily fabricated using conventional planar processes such as printed circuit board (PCB) or low-temperature co-fired ceramic (LTCC) method [3]. When used in a feeding network for antennas, SIW can improve the overall efficiency.

There are different types of antennas for different applications, for example microstrip antennas, slot antennas, and horn antennas. Microstrip patch antennas are very widely used. They are easy to fabricate and are compact, but with relatively narrow bandwidth and high loss, especially when the frequency goes up. For millimeter-wave applications, the dielectric resonator antenna (DRA) has been shown to be advantageous due to its low conductor loss and wide bandwidth.

1.2 Motivation

In typical communication systems, the receiving antenna is followed by a bandpass filter to reject the out-of-band noise and receive required information. In a conventional design,

antennas and filters are designed independently and then connected together through connectors. The input and output ports of both filters and antennas need to match with connectors, which introduces loss. The loss is even larger if mismatch happens. Matching transitions are added to eliminate the parasitic modes caused by discontinuities [4]. The whole design becomes complicated, large in size, and lossy. Also transitions added bring extra loss. The loss is generally proportional to frequency, so it becomes larger if operated in millimeter-wave frequency range.

Therefore filter and antenna integrations become attractive to improve the overall system performance. The general concept of filter and antenna integration is shown in Fig. 1.1. By removing the transitions between the filter and antenna, the loss is reduced and the design is more compact. In addition, the design time can be shortened because the interaction between components are more efficiently handled, with fewer device components.

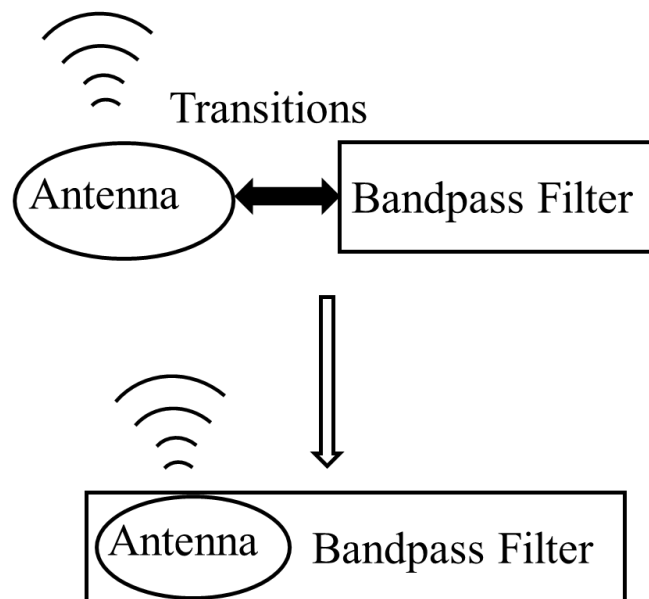


Fig. 1. 1. The general concept of filter and antenna integration.

An effective way to remove the transitions is to use the resonance characteristic of the antenna and couple it with the resonators of filter, which results in an extra order of the bandpass filter [5]. In other words, the last resonator and load of a filter are replaced by the antenna, but the function of the filter remains.

There have been studies on the antenna and filter integrations in the literature, mostly dealing with microstrip antennas and slot antennas. This subject has not been fully explored. In this thesis, two different types of filter and antenna integrations are studied.

1.3 Contributions

In this thesis, we focus on filter antenna integration design, including SIW filter and DRA integration, and microstrip filter and inset-fed microstrip patch antenna integration.

First, SIW filter and DRA integration in millimeter wave frequency range is presented. The DRA is integrated with SIW filter to form a compact design. High radiation efficiency is achieved. The design synthesis is presented, and the achievable Quality (Q)-factor range is studied. Moreover, integrations of the parasitic DRA and DRA array with SIW filters are implemented. The equivalent circuit and design curve of DRA array are discussed as well. All designs have been simulated and fine-tuned using full wave electromagnetic (EM) simulator. Preliminary measurement results are presented and tolerance analysis has been performed. To the best of our knowledge, there have not been reports on filter and DRA integrations or filter and antenna array integrations before this work.

In addition, the design of a microstrip bandpass filter integrated with patch antenna is also studied for improvement of coupling coefficient range. To increase the coupling value between the filter resonator and the antenna, the microstrip feed line of the patch antenna is directly connected to the filter. Simulation results show that, comparing to the reported values in the literature, a much larger range of coupling coefficient can be readily achieved using the direct connection. As a result, a wider design bandwidth can be realized.

1.4 Thesis Outline

Chapter 1 of the thesis provides an overview, motivation, and contributions.

In chapter 2, recent research advances have been reviewed on the filter antenna integrations. Different synthesis methods to achieve integration have been studied. Also, different types of integration are reviewed. Besides, the SIW technology is studied, which are very important for the design. Also, recent work on DRA is also reviewed to have a better understanding.

In chapter 3, we focus on the design of SIW filter and DRA and DRA array integration. The design process is explained in detail, and a number of examples are given. Equivalent circuit model is used to find out physical dimensions, and parameter extraction method is implemented to tune the designs. Integrations of single DRA, the parasitic DRA and DRA array with SIW filter, including coaxial-to-SIW transitions, have been designed and simulated using EM simulator. Simulation and measurement results are presented.

In chapter 4, integration of hairpin filter with inset-fed microstrip patch antenna is studied. It will be shown that using the direct coupled method between resonator of filter and patch antenna, a larger range of coupling coefficient can be achieved compared to the results in the literature.

In chapter 5, conclusions are drawn based on chapter 3 and chapter 4. Future work is discussed, including the improvement of the design performances.

CHAPTER 2

Literature Review

In this chapter, the work on integration of different types of filters and antennas integration is reviewed. Recent developments with DRA and SIW technology are also reviewed.

2.1 Filter and Antenna Integration

With the rapid development of wireless communication systems and satellite systems, more compact and low-profile devices are required. In conventional systems, filters and antennas are designed separately and then connected together, resulting in extra loss and degraded performance. Integration of filter and antenna gets rid of transition mechanism, making the whole structure lower loss, and more compact. In the review, different

methodologies of integration are reviewed, and various types of filter antenna integrations are presented.

Design methodology

There have been studies on the antenna and filter integrations, aiming to get rid of transitions and reduce total loss and overall sizes. In [6], the filter is directly inserted into the microstrip feed line of a patch antenna to have compact size. However, this design needs to have improved radiation efficiency, and a coupled line is required to do the matching between filter and antenna. In [7], filter and antenna are designed independently, with an impedance transmission line transition added between filter and antenna. This transition has a characteristic impedance higher than 50Ω , making it easier to match for filter. However, this design does not take some constraints into consideration, such as unbalanced configuration and transmission line technique, and it is hard to follow in other design environment as a general design synthesis.

These designs mentioned above still require transition structure between filter and antenna. There are studies devoted to getting rid of the transitions. The basic concept is that the antenna has the same resonant frequency as the filter center frequency, and the last resonator and load of the filter are replaced by the antenna. The antenna does two jobs simultaneously: the last resonator for the filter, and the radiator. Due to the replacement, there are two main considerations in the integration: coupling between antenna and resonator of filter, and load side external Quality (Q)-factor. The external Q -factor, Q_{ext} , of the filter needs to be consistent [8]. Besides the Q -factor, the coupling between the last resonator of the filter and antenna also needs to be with the same as a standalone filter.

A co-design method is proposed to integration filter and antenna [9-11]. This method of conventional coupled cavities synthesis for filters is implemented on filter antenna integration. The antenna is treated as one cavity resonator with radiation resistor, so the coupling between filter and antenna can be derived from asynchronous tuning coupling coefficient extraction [12].

In [13-16], another method is implemented. Equivalent circuit models are built to represent filters and antennas, so that the coupling between resonator and antenna can be derived from equivalent circuit model and related to physical dimensions. To be more specific, bandpass filters can be presented by series inductor and capacitor with impedance inverters K_{ij} , as indicated below [17].

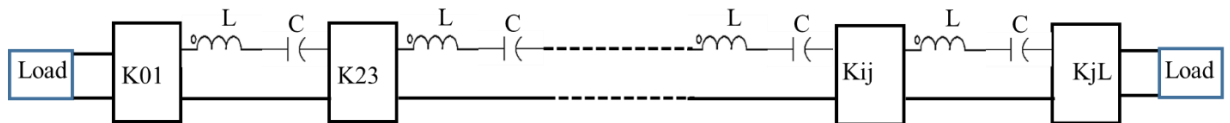


Fig. 2. 1. Equivalent circuit model of bandpass filter with impedance inverter.

Also, the equivalent circuit model of antenna can be represented by series RLC circuits [18]. As a result, the coupling between the last resonator of filter and antenna can be derived from the equivalent circuit model based on parameter extraction using full-wave simulation.

In this thesis, the SIW filter and DRA integration adopts the method of building equivalent circuit models. The design synthesis follows the general steps in [19].

Different types of filter-antenna integration

Reported filter-antenna integrations in the literature deal mostly with microstrip antennas [20-25], and slot antennas [26-28].

Microstrip antennas are widely used in microwave application due to their low-profile, ease of fabrication and low cost. In [20], a microstrip antenna and filter integration is presented. However the coupling between patch antenna and filter resonator is not well explained. A co-design of coplanar waveguide filter and circular patch antenna is presented in [21]. The patch antenna replaces the last resonator and one port of filter, so the whole design is integrated and planar. In [22-24], patch antenna and Substrate Integrated Waveguide (SIW) filter are integrated. Both stacked and cascaded approach are implemented but the design syntheses are not given. A hairpin bandpass filter and microstrip patch antenna using filter synthesis approach is given in [25]. The antenna is proximity coupled to the resonator of the filter to form the integration. However, the proximity coupling method has fabrication limitation when the patch antenna and the resonator are close to each other. In this thesis, the direct coupled method is used to directly connect feeding microstrip line of the patch antenna to the resonator of a bandpass filter. A much larger achievable coupling range can be achieved.

In [26], [27] SIW filters are integrated with slot antennas to achieve high system efficiency. In [28], cavity-backed slot antenna is integrated with stacked SIW filter in order to reduce the cross-polarization and improve the gain. But the achievable bandwidth is narrow.

In this thesis, we focus on the dielectric resonator antenna (DRA) integration with SIW filter, which, to the best of our knowledge, has not been investigated. We further investigate the integration with antenna array and with parasitic antenna.

2.2 Dielectric Resonator Antenna (DRA)

The millimeter wave range has attracted a lot of attention for many different applications, which remains to be fully investigated compared to well-used lower frequency range. For example, the satellite system popularity brings demand for large bandwidth antennas. Traditional planar antennas suffer from narrow bandwidth, power loss and decayed radiation efficiency.

The DRA is very attractive for millimeter wave applications due to its low conductor loss, high radiation efficiency in high frequency range [29], [30]. Also, DRA achieves wider bandwidth than microstrip antennas, and smaller size than horn antennas.

The DRA can be implemented in different shapes, such as rectangular [31], cylinder [32], or hemisphere [33]. It can be excited through different feeding methods, such as coaxial probe feeding [34], [35], microstrip line feeding [36], and coplanar waveguide feeding [37]. Many feeding mechanisms suffer from high feeding loss in millimeter wave frequency range. A rectangular waveguide feeding method is used in [38] with low loss. However, it is expensive and bulky, which makes it difficult to fabricate and for mass production. A rectangular DRA model excited by rectangular waveguide is shown in Fig. 2.2. Port to external load is placed on one side of the rectangular waveguide, while the other side is short circuited.

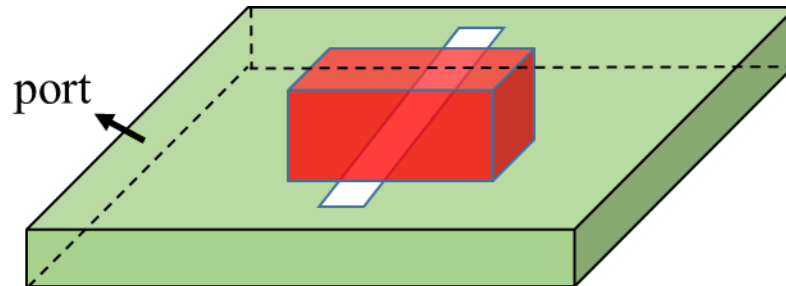


Fig. 2. 2. Schematic of rectangular DRA fed by rectangular waveguide.

2.3 Substrate Integrated Waveguide

The substrate integrated waveguide (SIW) is very promising for millimeter wave applications. The SIW is formed using two rows of metalized via holes inside a dielectric substrate with top and bottom metal plates. Due to the planar structure, the SIW can be easily integrated with other coplanar or microstrip circuits with simple transition. It can be fabricated using standard printed circuit board (PCB) process, which is widely used and low cost. SIW provides good alternative for traditional air-filled rectangular waveguide and microstrip line. SIW has less radiation loss and better quality factor than conventional planar circuits. It is also easier to fabricate and more compact than the traditional rectangular waveguides.

The concept of SIW structure was first brought up in 1994 [39]. The configuration is shown in Fig. 2.3. Integration of microstrip line and SIW is investigated in [40]. The dispersion and propagation characteristics of SIW are analysed in [41], [42]. Different methods are used to model and analyse the structure, such as method of moments (MoM), eigenvalue equations, and surface impedance methods [43-45]. Design rules and overall comparative studies are presented in [46] and [47].

In X-band or higher working frequency, SIW works efficiently due to the compact sizes and low loss. However, in the lower frequency, SIW suffers from relatively large width. In [48], a metal strip and two more rows of vias are inserted to implement the SIW at lower frequency.

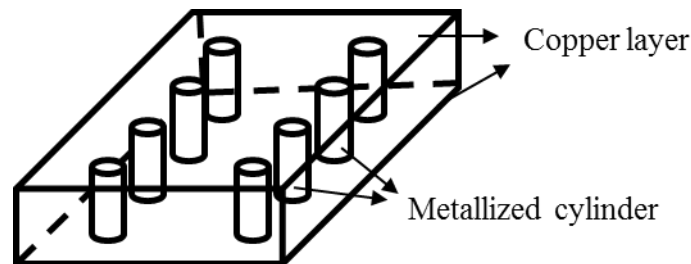


Fig. 2. 3. Model of SIW, with two rows of via holes.

Since the design rules and wave propagation studies of SIW have been presented, many practical applications are implemented in microwave and millimeter wave applications,

such as filters, antennas, resonators, and amplifiers. SIW filters can be stacked [49] or cascaded [50], [51] based on different usages.

Many devices have been built based on SIW with high performance. In [52], a super-wide filter is investigated using SIW and periodic structure integration. The SIW cut-off characteristic improves the performance of the filter. The SIW filters brings the advantages of low insertion loss, and high quality factor [53], [54]. When SIW is utilized for amplifiers, relatively lower loss is observed compared to traditional microstrip lines [55].

Antennas based on SIW feeding mechanism have many advantages. Beside the fact that it can be easily fabricated using PCB technology, SIW can reduce loss and increase the radiation efficiency consequently. By replacing the expensive rectangular waveguide, the SIW reduces the cost and achieves high radiation efficiency and wide band when it is integrated with the cavity-back antenna in [56]. SIW structure has also been employed as a feeding method for DRA in [57-59].

In this thesis, the SIW structure is used to build bandpass filter, and the feeding mechanism for DRA and DRA array.

CHAPTER 3

Integration of DRA and SIW Filter

In this chapter, the theory and design of SIW filter and DRA integration are presented. First, the individual designs of SIW filter and DRA are explained. The integration procedure is then presented in detail, including the method for tuning of the integrated structures.

We consider the integration of SIW filter with single DRA, parasitic DRA, and DRA array, respectively. Design examples and full wave simulations are provided for verifications. Preliminary experimental results are also presented.

3.1 Design of SIW Filter

To design an SIW filter, the dimensions of SIW needs to be calculated first. Instead of walls, the SIW has metalized vias with certain distance between each other. As a result, the leakage and dispersion characteristics need to be taken into consideration when calculating the cut off frequency and width. The behavior of SIW is similar to a rectangular waveguide with an equivalent width [41]. The formula to calculate the cut off frequency of SIW is given below under the TE₁₀ mode [41].

$$f = \frac{c}{2\pi\sqrt{\epsilon_r}} \sqrt{\left(\frac{\pi}{a_{eff}}\right)^2} \quad (3.1)$$

where c is the speed of light. a_{eff} is the equivalent width and can be derived from the parameters below [41]:

$$a_{eff} = a_{SIW} - \frac{d_{via}^2}{0.95 * p_{via}} \quad (3.2)$$

where a_{SIW} is the distance between two rows of vias, d_{via} is the diameter of each via, and p_{via} is the distance between two adjacent vias.

Also, to avoid radiation loss and leakage from gaps between adjacent cylinder vias, two constraints are applied when selecting the dimensions [41, 42]:

$$d_{via} < 0.2 * \lambda_g \quad (3.3)$$

$$d_{via} \geq \frac{p_{via}}{2} \quad (3.4)$$

where λ_g is the guided wavelength in SIW. These two constraints ensures radiation loss can be negligible. Note that these two constraints are sufficient but not necessary.

After the basic parameters of substrate are decided, a bandpass Chebyshev filter can be designed based on the substrate. The standard procedure to build Chebyshev bandpass filter is followed [17]. First of all, a lowpass prototype filter is needed to realize the transfer function. Element values g_i are normalized to have cutoff frequency Ω_c equal to 1, and the source resistance or conductance g_0 equal to 1, as well. Element values for a 4-pole Chebyshev prototype filter are given by [12]:

$$g_0=1, g_1=0.9314, g_2=1.292, g_3=1.5775, g_4=0.7628, g_5=1.221$$

where g_n represents shunt capacitance or series inductance, and g_{n+1} is the load resistance or conductance. Then, the fractional bandwidth FBW is given by:

$$FBW = \frac{f_2 - f_1}{f_0} \quad (3.5)$$

where f_2 and f_1 defines the passband, and f_0 is the center frequency.

Having obtained the prototype parameters and fractional bandwidth, the bandpass filter design parameters can be derived from:

$$Q_{ext} = \frac{g_0 g_1}{FBW} = \frac{g_4 g_5}{FBW} \quad (3.6)$$

$$k_{ij} = \frac{FBW}{\sqrt{g_i g_j}} \quad (3.7)$$

where Q_{ext} is the external Q-factor of the filter, which represents coupling between last resonator to output/input, and k_{ij} is the inter-resonator coupling coefficient between adjacent resonators.

Without losing generality, an example of SIW filter is designed at a center frequency of 35.5 GHz. The 3D model is shown in Fig. 3.1. This four-pole bandpass filter will be

compared with the filter antenna integration later. The fractional bandwidth is 5.6% and the design parameters are shown below:

$$k_{12}=0.051, k_{23}=0.039, Q_{\text{ext}}=16.63$$

Top view of the SIW filter model is showed in Fig. 3.2, with design parameters. L_n ($n=0, 1, 2$) control coupling coefficients, and W_n ($n=1, 2$) denotes the length of resonators, and this length is around half wavelength.

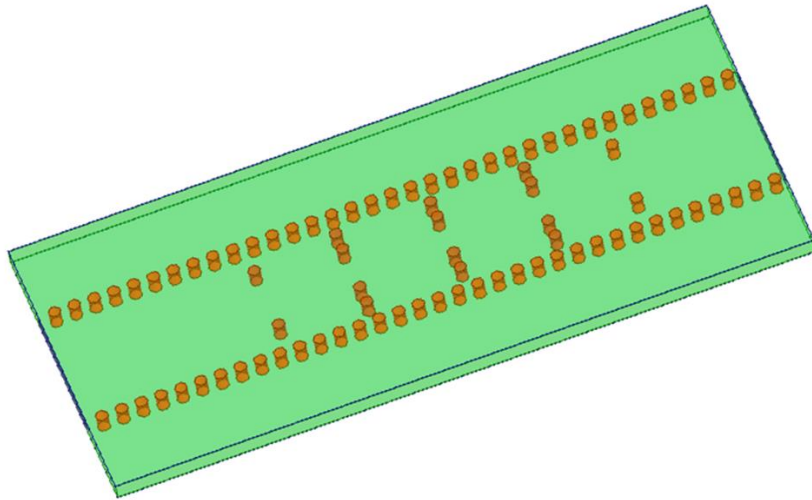


Fig. 3. 1. 3D model of SIW four-pole bandpass filter.

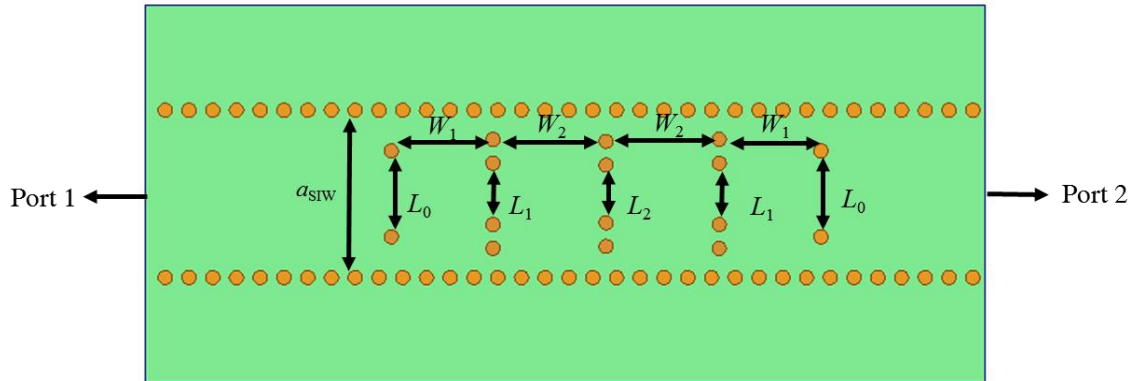


Fig. 3. 2. Top view of the four pole SIW filter ($a_{SIW}=4.5$ mm, $L_0=2.032$ mm, $L_1=1.384$ mm, $L_2=1.27$ mm, $W_1=2.326$ mm, $W_2=2.64$ mm).

The structure will be built using *RT/Duroid 6002* substrate with a thickness of 20 mil, covered with 17- μm -thick bottom and top copper layers. The dielectric constant ϵ_r is 2.94 and loss tangent $\tan\delta=0.0014$. The SIW has a width $a_{SIW} = 4.8$ mm, and the diameter of via $d_{via} = 0.38$ mm with the separation $p_{via} = 0.64$ mm, as indicated in Fig. 3.3.

The ideal filter responses (the S-parameters) are shown in Fig. 3.4.

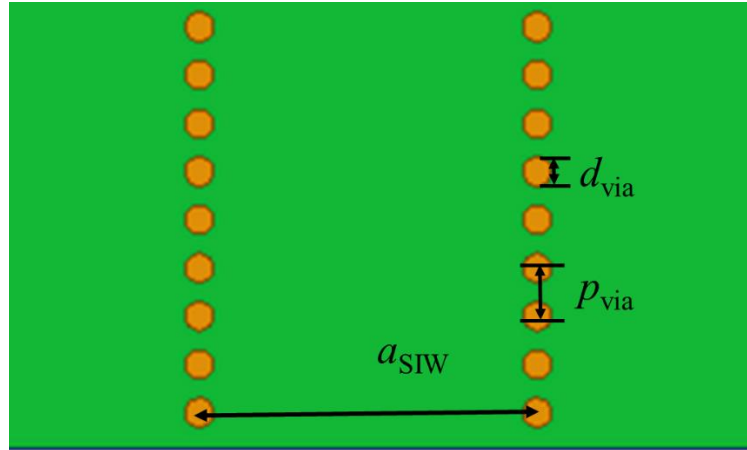


Fig. 3. 3. The parameters of SIW.

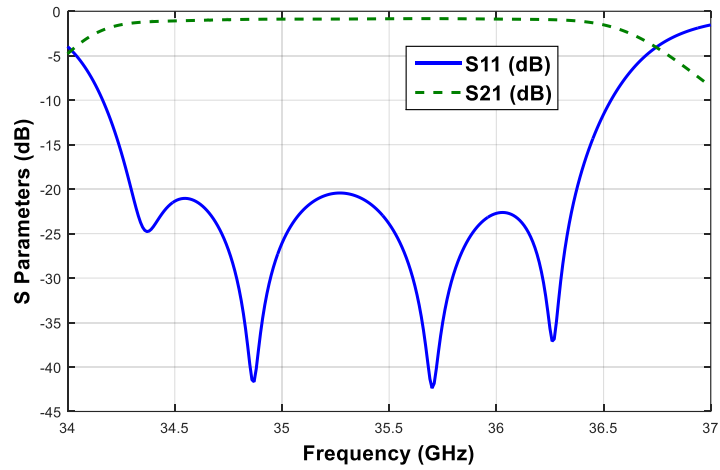


Fig. 3. 4. The S parameters of the four-pole filter.

Equivalent Circuit Model and Tuning of SIW Filter

In the thesis, parameter extraction method [62] is used to optimize the design. The detailed analysis will be given in section 3.4. A brief introduction is shown in this section to tune the filter. The filter is tuned using a coarse model and a fine model. An equivalent circuit model built in Keysight ADS is adopted as a coarse model. The fine model is built using Ansoft High Frequency Structure Simulator (HFSS). The coarse model is used to assist the tuning of the structure in the fine model, which is accurate but time-consuming.

First of all, the equivalent circuit model for SIW filter needs to be built. As we know, the SIW can be seen as rectangular waveguide with an equivalent width. SIW cavities of a filter are half-wavelength transmission lines. The coupling between adjacent cavity resonators is treated as ideal impedance K inverter [60]. The K inverter is represented using $ABCD$ matrix, and half-wave transmission lines are represented in S matrix. Note that all characteristic impedances are normalized to $Z_0=1$.

The relationship between the SIW filter and its equivalent circuit model is shown in Fig. 3.5. A section of the equivalent circuit model built in ADS is shown in Fig. 3.6, showing the first two cavities.

The equations to calculate K-inverter are given below [17]:

$$K_{01} = \sqrt{\frac{\pi\Delta\lambda}{2g_0g_1}} K_{4L} = \sqrt{\frac{\pi\Delta\lambda}{2g_4g_5}} \quad (3.8)$$

$$K_{ij} = \frac{\pi\Delta\lambda}{2\sqrt{g_i g_j}} \quad (3.9)$$

where K_{ij} is the impedance inverter. $\Delta\lambda$ can be calculated using

$$\Delta\lambda = \frac{\lambda_{g1} - \lambda_{g2}}{\lambda_{g0}} \tag{3.10}$$

where λ_{g1} and λ_{g2} denoted the wavelengths at the band-edge frequencies, and λ_{g0} is the guided wavelength at the center frequency.

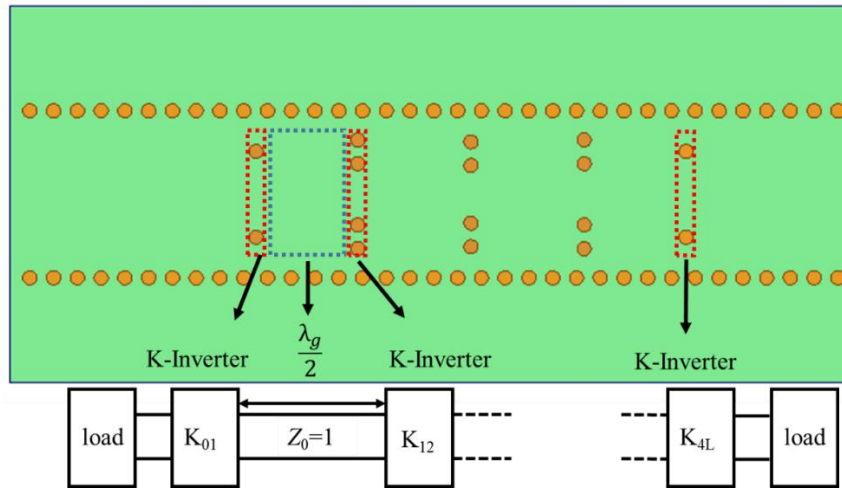


Fig. 3. 5. The generation of equivalent circuit model of SIW filter.

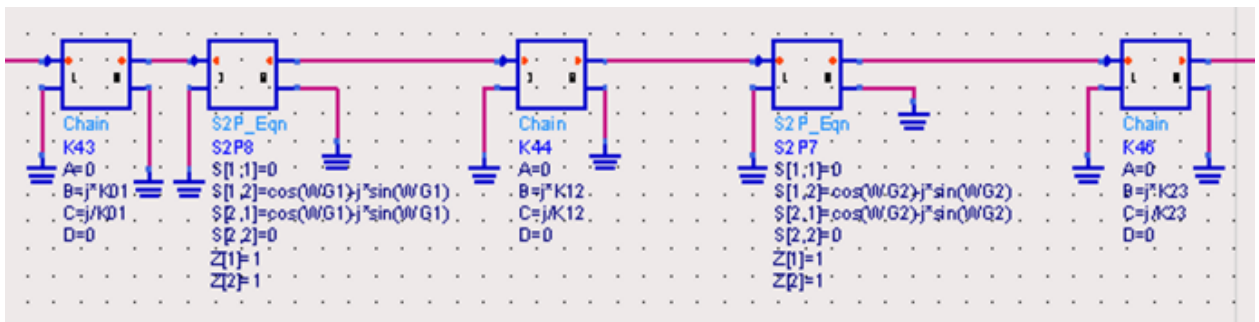


Fig. 3. 6. The schematic of equivalent circuit model in ADS, showing the first two cavities.

Then, the fine model responses from HFSS are compared with the coarse model in ADS. Parameters, such as K values, are extracted and compared with the ideal parameters in the coarse model. Instead of tuning of the fine model in HFSS directly, the coarse model provides the corresponding adjustments in fine model and guides the tuning of the fine model.

When optimizing the parameters, the widths L_0 , L_1 , and L_2 control the coupling K inverter values. If the width needs to be enlarged, the length of the cavity resonator needs to be reduced accordingly. This is due to that fact that when iris width becomes larger, the resonant frequency of the cavity shifts to lower frequency. Therefore the length needs to be reduced to compensate for the frequency shift.

Fig. 3.7 shows the final tuned filter responses and good agreement is achieved between the coarse model in ADS and the fine model in HFSS.

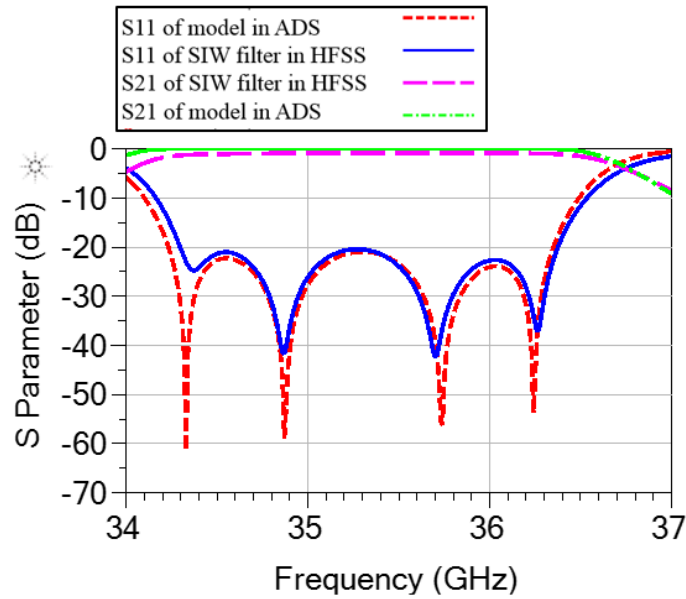


Fig. 3. 7. S-parameters of equivalent circuit model in ADS and the SIW filter design in HFSS.

3.2 Design of Dielectric Resonator Antenna

The DRA is a good candidate for millimeter wave applications. Design involves considerations of both the antenna, a rectangular DRA, and the feeding structure. SIW is adopted as the feeding mechanism for DRA, which helps to reduce loss, and a slot on top of the SIW is used to excite the desired mode in DRA.

DRA is designed to have the same resonant frequency as the filter center frequency. The equations of DRA dimensions are given in [29] as shown below:

$$k_x = \frac{\pi}{a_{DRA}}, k_z = \frac{\pi}{2h_{DRA}} \quad (3.11)$$

$$k_y \tan\left(\frac{dk_y}{2}\right) = k_0 \quad (3.12)$$

where $k_0^2 = k_x^2 + k_z^2$ and k_0 is the free space wavenumber corresponding to the resonant frequency. The DRA will be made using *Rogers RT6010*. Given the thickness of 50-mil and the dielectric constant $\epsilon_r = 10.2$, different groups of DRA dimensions can be calculated. The dimensions used in this thesis are given in Fig. 3.8.

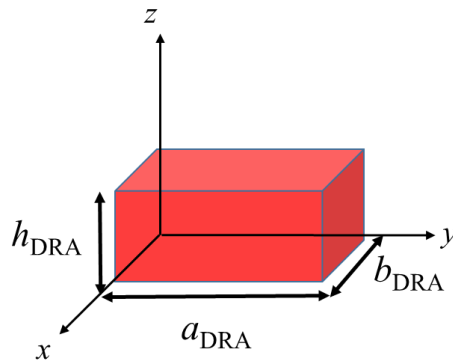


Fig. 3. 8. DRA dimensions ($a_{DRA} = 3 \text{ mm}$, $b_{DRA} = 1.5 \text{ mm}$, and $h_{DRA} = 50 \text{ mil}$).

The SIW is used as feeding mechanism for the DRA. The dimensions for the SIW is the same as the SIW filter design in the previous section. A slot is used to strongly excite the mode, which is etched on the top plate of SIW at the strongest field. The position of slot is initially selected at $\lambda_g/2$ from the short circuit (λ_g is the guided wavelength inside SIW), where the maximum excitation locates. The design of SIW based DRA is given in Fig. 3.9 with dimensions.

The full wave electromagnetic (EM) simulated S_{11} and radiation pattern of DRA design are shown in Fig. 3.10.

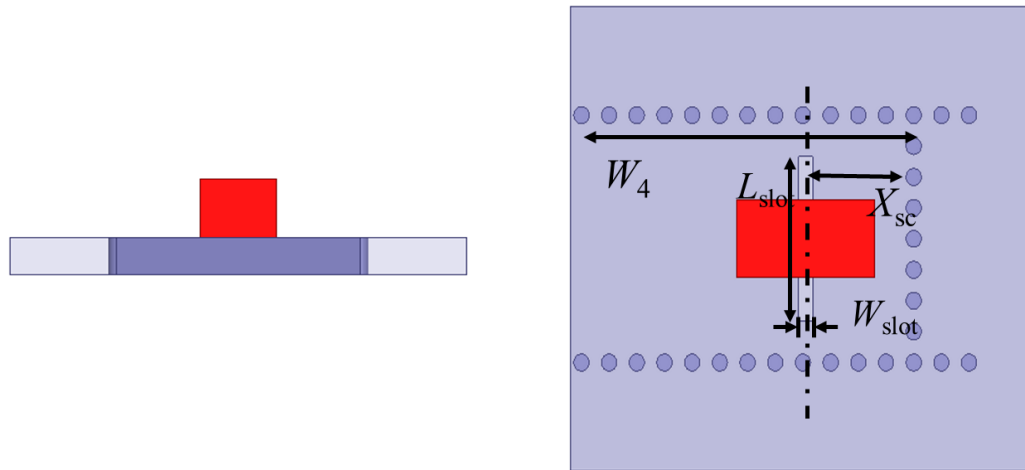
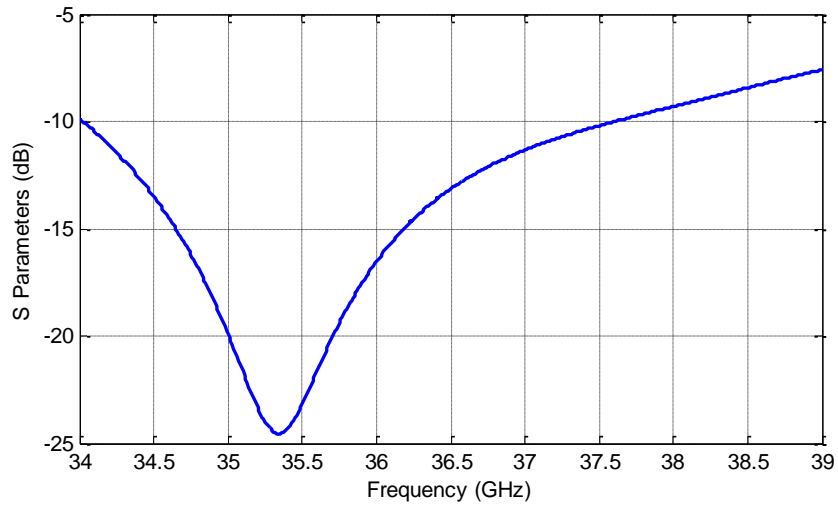
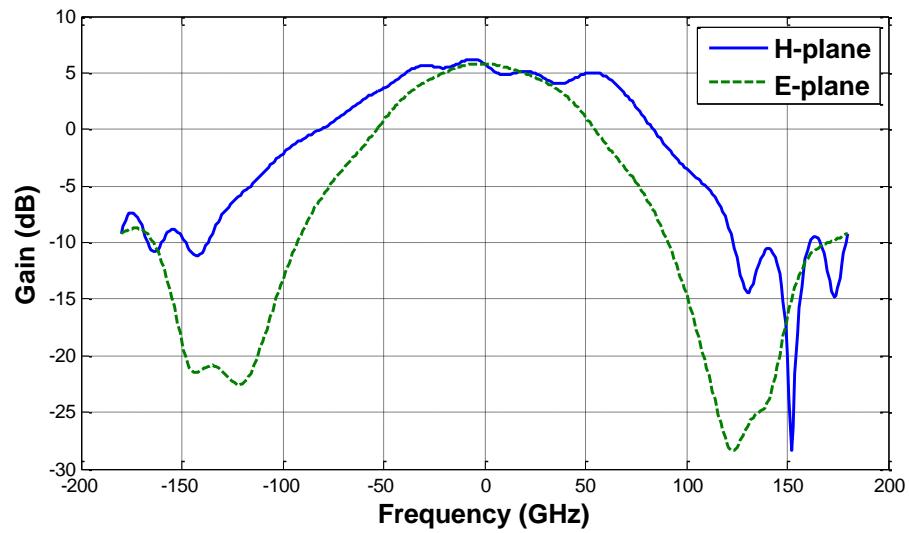


Fig. 3. 9. The top view and side view of SIW-based DRA ($L_{slot} = 3.2 \text{ mm}$, $W_{slot} = 0.3 \text{ mm}$, $X_{sc} = 3.5 \text{ mm}$, $W_4 = 4.9 \text{ mm}$).



(a)



(b)

Fig. 3. 10. The EM simulation results of SIW-based DRA structure: (a) $|S_{11}|$ and (b) radiation pattern.

3.3 Filter Antenna Integration

To achieve a filter antenna integration, the last resonator and the load is replaced by the DRA. In this section, we follow the design principle presented in [61].

The DRA needs to keep the characteristic of a radiator, and act like a resonator for the filter simultaneously. The configuration of filter antenna integration is shown in Fig. 3.11 and Fig. 3.12. The SIW filter and DRA designed in previous sections are used as reference for integration. The DRA is directly mounted on the top of SIW, with a slot etched for excitation. The integrated design has three SIW cavities and the DRA. The DRA and the section of SIW underneath together behave like the last resonator and the load.

For the integrated design to have similar behavior as the four-pole bandpass filter, the coupling between the third resonator and the DRA needs to be the same as k_{34} in the four-pole filter. In addition, Q_{ext} , the external coupling coefficient of the filter should remain the same for the integrated design.

Synthesis procedure is presented next following the flow chart in Fig. 3.13.

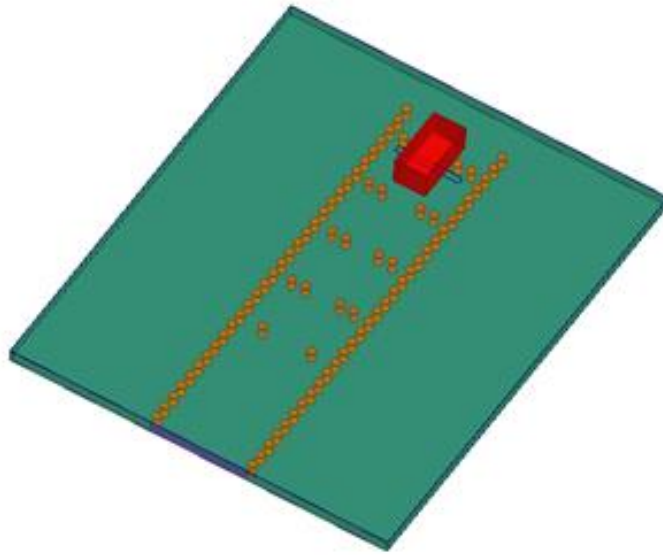


Fig. 3. 11. 3-D model of SIW filter and DRA integration.

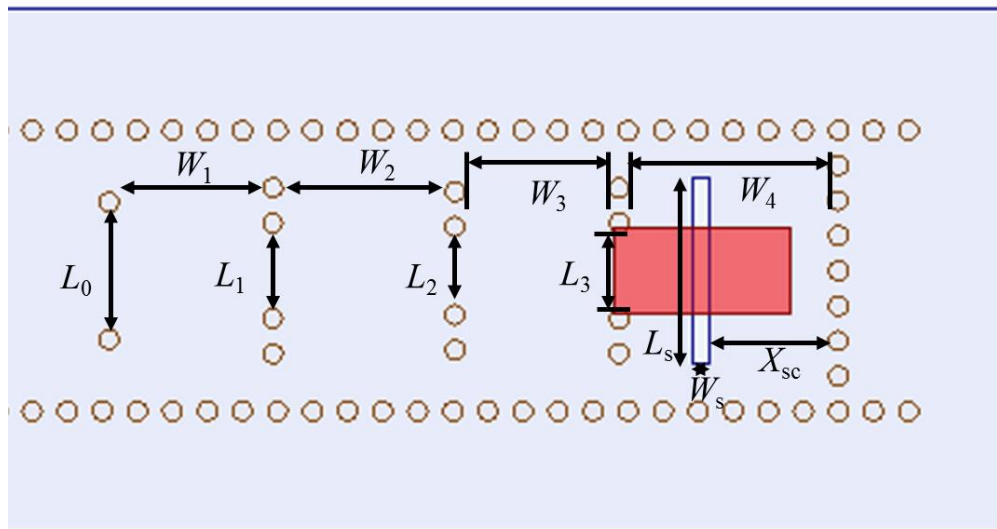


Fig. 3. 12. Top view of filter antenna integration ($L_0=2.032$ mm, $L_1=1.384$ mm, $L_2=1.27$ mm, $L_3=1.5$ mm, $W_1=2.326$ mm, $W_2=2.64$ mm, $W_3=2.6$ mm, $X_{sc}=0.93$ mm, $W_4=2.49$ mm, $L_s=3$ mm, $W_s=0.3$ mm).

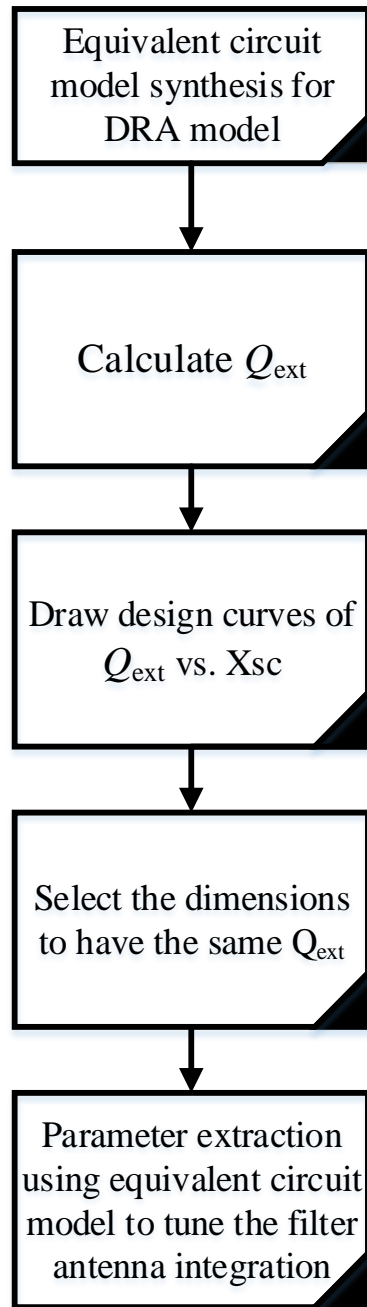


Fig. 3. 13. Flow chart for filter antenna integration.

Extraction of Q_{ext}

The structure of DRA fed by SIW with one end short-circuited can be modeled as the equivalent circuit model in Fig. 3.14. The phase of S_{11} , and the real and imaginary parts of the input impedance of the structure in Fig. 3.14 are simulated and compared in Fig. 3.15. It proves that within the bandwidth the behaviors of the DRA and the equivalent circuit are similar.

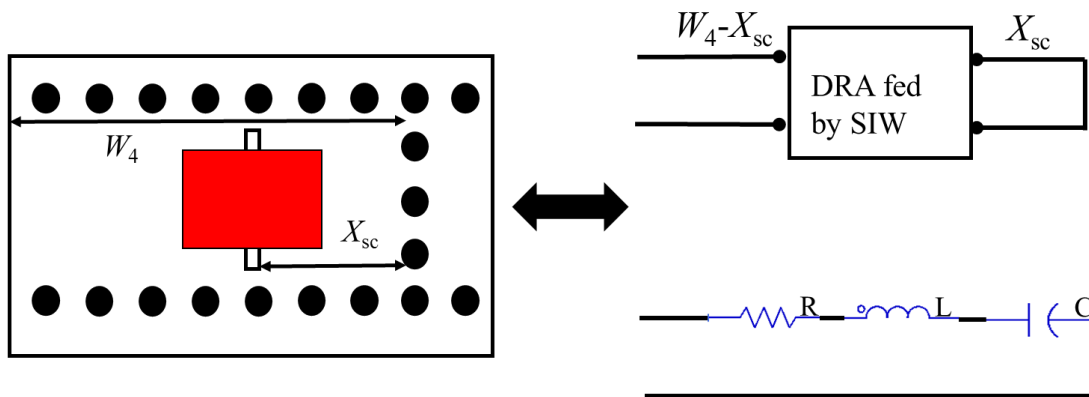
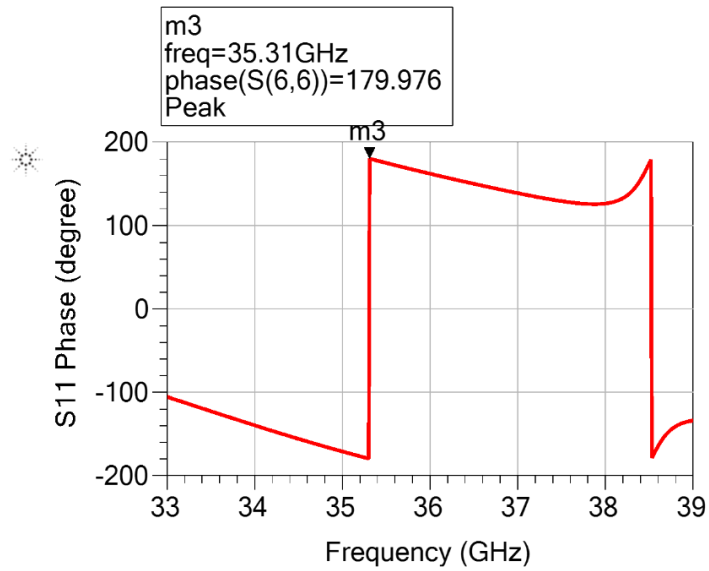
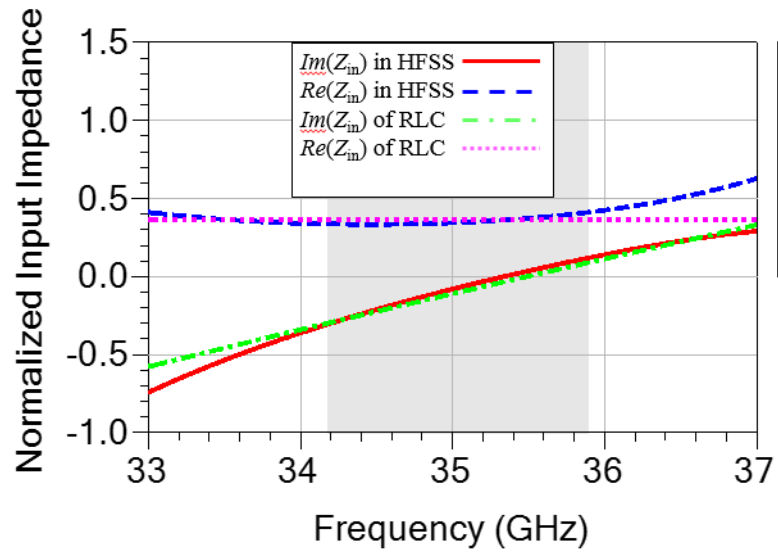


Fig. 3. 14. Configuration of DRA and its equivalent circuit model

That is to say, the DRA can be modeled as a series RLC circuit within the bandwidth. At the resonance frequency, the phase of S_{11} of series RLC circuit is 180° , as indicated in Fig. 15(a). This characteristic is used to determine the length of transmission line W_4 .



(a)



(b)

Fig. 3. 15. (a) Phase of S_{11} and (b) the normalized input impedance of the design in HFSS and the equivalent RLC circuit.

To calculate the Q_{ext} of DRA, the input impedance is simulated and compared with a series RLC circuit, as shown in Fig. 3.15(b). The external Q factor Q_{ext} can be calculated using the equations for series RLC:

$$Q_{\text{ext}} = \frac{\omega_0 L}{R} \quad (3.13)$$

where

$$L = \frac{d(\text{Im}(Z_{\text{in}}))}{2d\omega} \Big|_{\omega=\omega_0}, R = Z_{\text{in}}(\omega_0) \quad (3.14)$$

Design curve of Q_{ext} vs. X_{sc} and L_s

To find out the variation of Q_{ext} , the dimensions that affect the Q factor need to be found.

The surface current is the strongest at the short circuit, and it again reaches the maximum at $\lambda_g/2$ from the short circuit, where the strongest coupling happens. As a result, the distance X_{sc} affects the Q_{ext} of DRA by varying the coupling. Moreover, the slot length L_s also affects the Q_{ext} . The slot length varies the excitation from SIW to DRA, leading to shifts of resonant frequency. If the bandwidth of DRA is wider than the filter, a shift in resonant frequency of DRA can still cover the required bandwidth, and the coupling between cavity and antenna still works. This broad bandwidth provides more flexibility when integrating the filter and antenna.

Therefore, by varying the distance X_{sc} and L_s , an achievable range of Q_{ext} can be derived and the design chart of Q_{ext} vs. X_{sc} and L_s is presented in Fig. 3.16. The range of Q_{ext} is found to be at least 9-100, which corresponds to a bandwidth range 1%-11%.

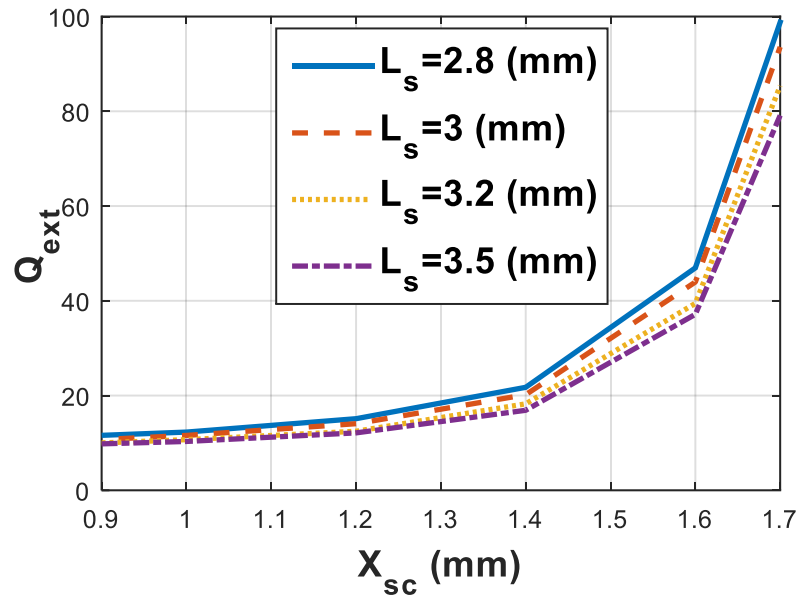


Fig. 3. 16. The design curve of Q_{ext} vs. X_{sc} and L_s .

Dimension selection

Due to the broader bandwidth of DRA, different combinations of X_{sc} and L_s can be used to get the same Q_{ext} . In this case, the value of X_{sc} and L_s are selected as 1.3 mm and 3.2 mm. The cavity length W_4 is selected to have the phase of S_{11} equal to 180° at the center frequency, and the value is 4.5 mm.

3.4 Tuning of the Structure

The parameter extraction in space mapping [62] is applied to tune the structure. The fine model, which is based on the full wave solver HFSS, is accurate but time-consuming. Therefore a coarse model is implemented to assist the optimization process. The coarse

model is fast but not very accurate. The goal is to achieve optimized design of the fine model without directly optimizing it. Instead, the coarse model is used to guide the optimization of the fine model. First, data from fine model is compared to the coarse model. The parameters in the coarse model are tuned so that the responses closely match the output from the fine model, which is referred to as parameter extraction. After that, the extracted values are compared to the ideal coarse model parameters, and a new prediction is made in fine model to get better results, i.e. shifts in certain variables. So the dimensions in HFSS are adjusted to get new responses and the first iteration is finished. If the responses meet design specifications, the optimization stops. Otherwise the next iteration starts.

The equivalent circuit model of filter antenna integration built in Keysight ADS serves as the coarse model. The SIW-fed DRA section is modeled using a combination of EM simulated DRA and two waveguide sections, as shown in Fig. 3.17 and Fig. 3.18. The DRA is simulated with two ports de-embedded to the center of the antenna. Note that a small section of transmission line with length ΔX_{sc} as shown in Fig. 3.18 is added next to the short circuit to count for the fact the via wall is not a perfect short-circuit.

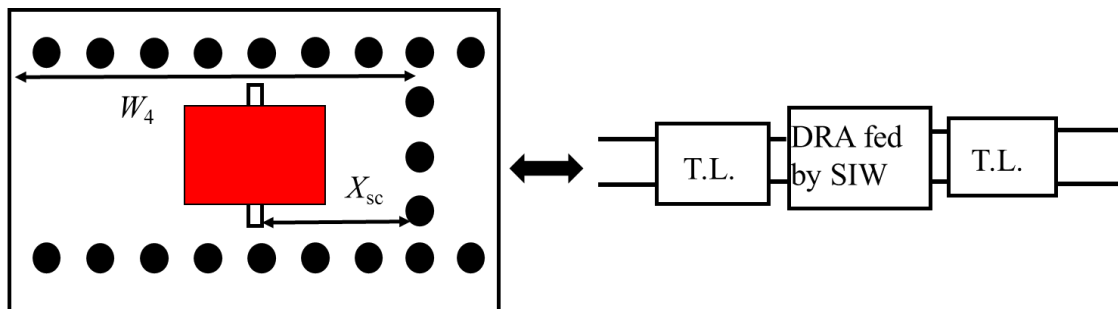


Fig. 3. 17. The equivalent circuit for DRA.

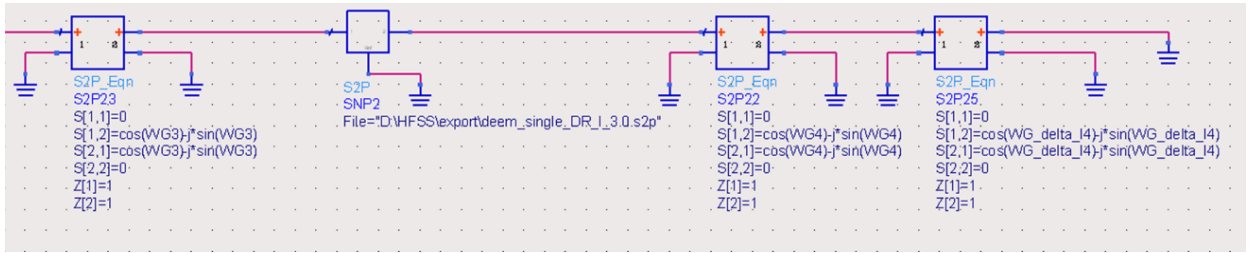


Fig. 3. 18. Equivalent circuit model of SIW-fed DRA in ADS.

The complete equivalent circuit model for the filter antenna integration is shown in Fig. 3.19(b). The filter model is shown in Fig. 3.19 (a) for comparison. Transmission lines are used to equivalently represent SIW cavities as mentioned in section 3.1. K -inverters model the inter-cavity coupling and they are normalized to characteristic impedance $Z_0=1$. The last resonator and load of SIW filter are replaced by the DRA equivalent circuit model.

Simulated $|S_{11}|$ of the filter antenna integration before optimization is shown in Fig. 3.20. Using the coarse model in ADS and the fine model in HFSS, the design is finely tuned following the parameter extraction process explained. After a few iterations, good return loss is achieved over the passband as shown in Fig. 3.21.

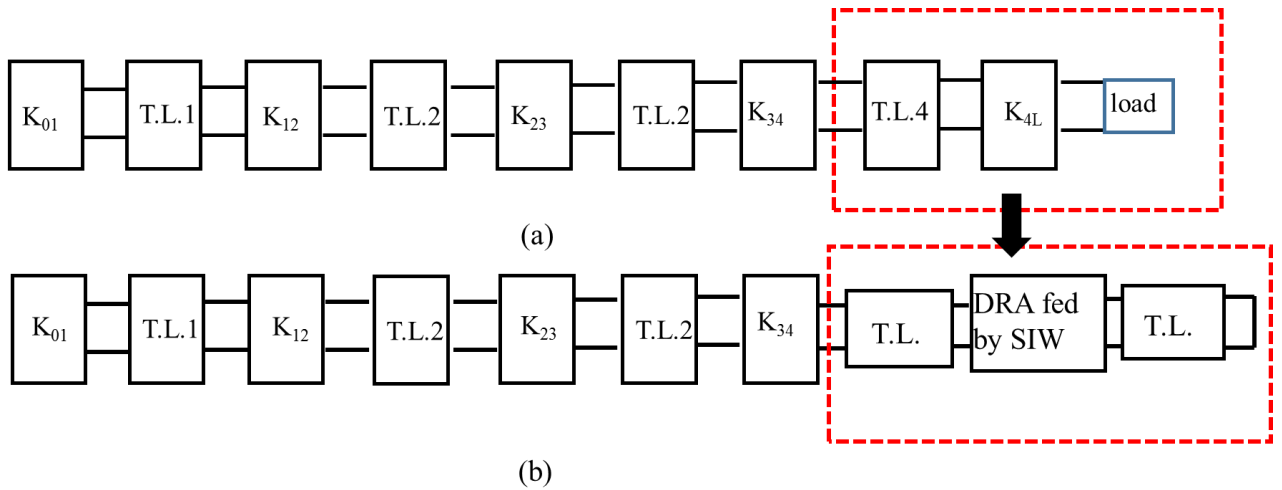


Fig. 3. 19. The equivalent circuit models for (a) SIW filter and (b) filter antenna integration.

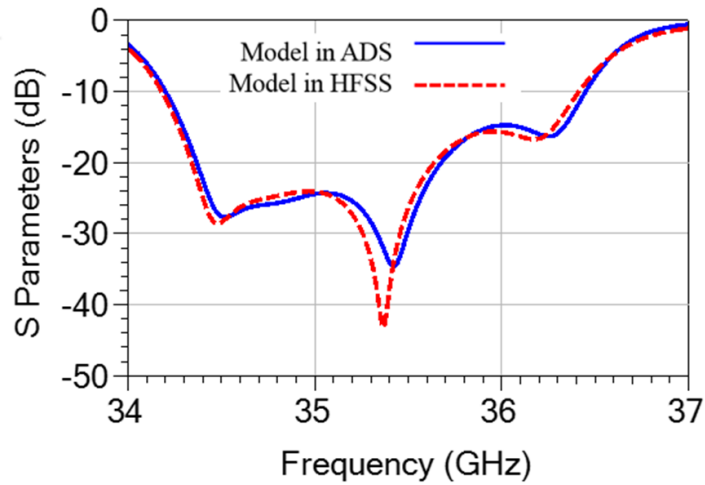


Fig. 3. 20. Simulated $|S_{11}|$ of the filter antenna integration before optimization.

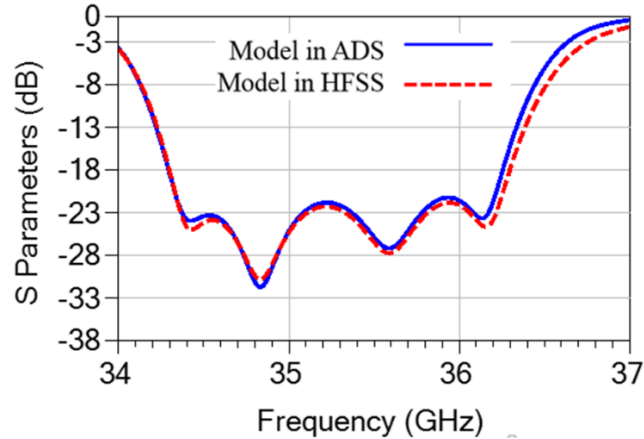


Fig. 3. 21. Simulated $|S_{11}|$ of the filter antenna integration after fine tuning.

Parameter tuning discussion

A comparison between SIW filter and filter DRA integration is made. The coupling iris length between the third resonator and DRA, L_3 , is increased from 1.384 mm for the filter, to 1.5 mm for the integrated design. This length denotes the K-inverter value K_{34} increases for filter and antenna integration.

As shown in Fig.3.22, bandpass filters can be assumed as lossless LC circuits with coupling inverters between them [12]. Note that, in section 3.1, the cavities are assumed to be transmission lines. These two models are both equivalent circuit models for bandpass filter, but with different applications. In section 3.1 Fig. 3.5, the equivalent transmission line is used to represent physical dimensions of cavity lengths. In this section Fig. 3.22, inductance and capacitor are used instead.

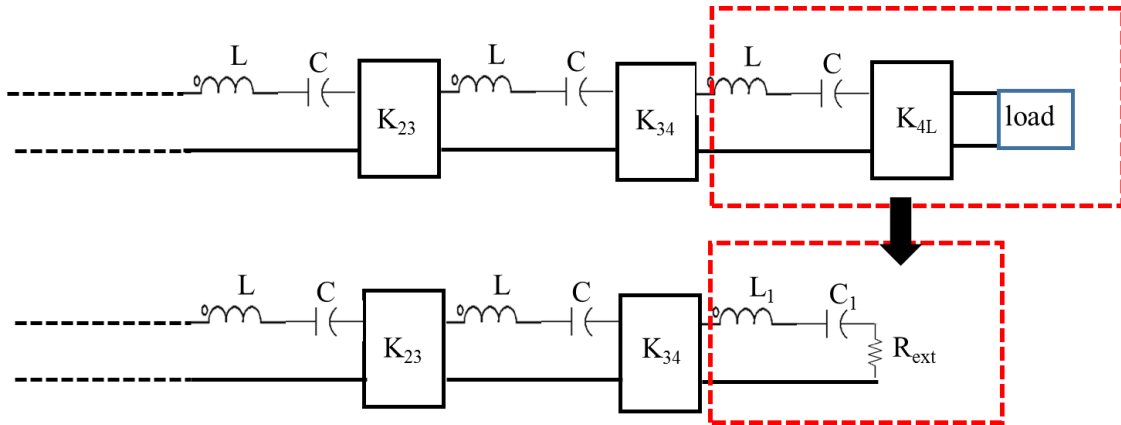


Fig. 3. 22. Equivalent circuit model for bandpass filter and filter antenna integration.

The length from DRA to the short circuit, X_{sc} , changes the input impedance of the DRA and the feeding section, and consequently, it affects the slope of input impedance, which leads to change in inductance value L_1 .

$$k_{34} = \frac{K_{34}}{2\pi f_0 \sqrt{L_1 L}} \quad (3.15)$$

With the equation (3.15), the k_{34} needs to be consistent to keep filter characteristic, while L_1 varies with different X_{sc} lengths. Therefore, the K -inverter K_{34} needs to change correspondingly to compensate for the change of L_1 . It is observed that when X_{sc} becomes smaller, L_1 becomes larger, so K_{34} needs to be increased so that k_{34} remains.

3.5 Coaxial to SIW Transition

For the integrated design to be built and tested, a coax-to-SIW transition is designed. It consists of two matching vias inside the substrate, and a short circuit made of vias. A circle

is etched on the bottom plate of SIW for excitation. A back-to-back structure shown in Fig. 3.23 is designed. This structure consists of two symmetric coax-to-SIW transitions with a distance much larger than λ_g between them, as indicated in Fig. 3.24. S_{11} of the back-to-back structure is optimized using HFSS, so that $|S_{11}|$ is at least less than -25 dB over the bandwidth of interest. Once properly designed, the transition will not significantly affect the reflection coefficient when it is added to the main design. The two large cylinders that are mounted on both sides of the transitions are for fabrication assembly alignment and they do not affect simulation results.

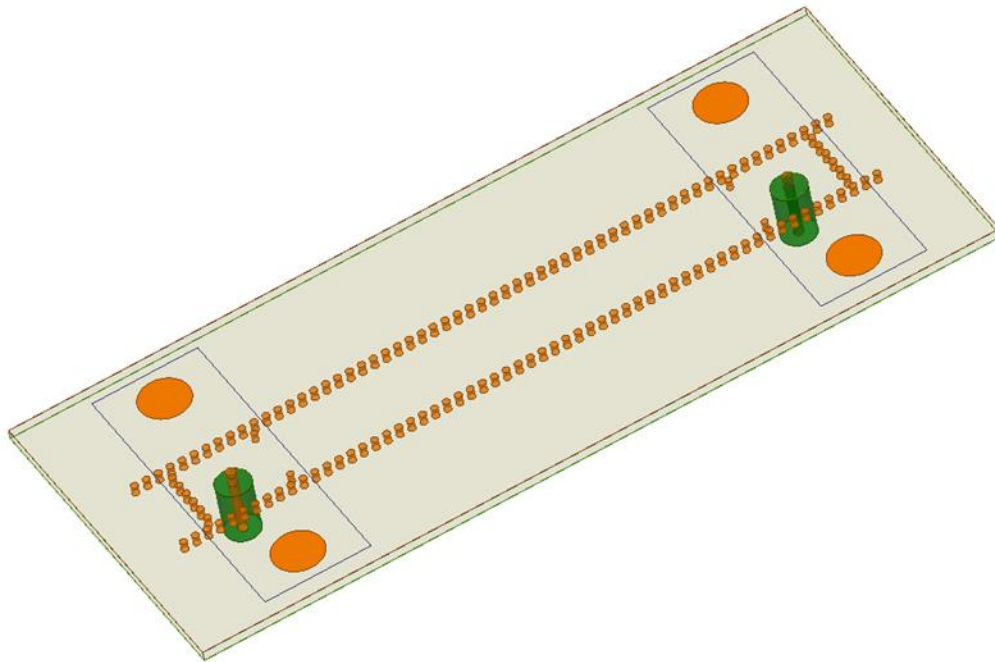


Fig. 3. 23. 3-D model of back-to-back coax-to-SIW transitions.

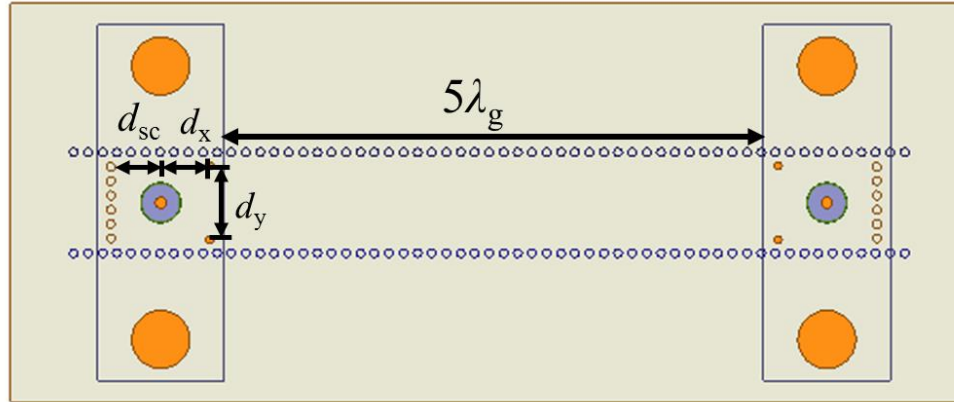


Fig. 3. 24. Top view of the back-to-back coax-to-SIW transitions ($d_{sc}= 2.3$ mm, $d_x= 2.18$ mm, $d_y= 3.35$ mm).

The effects of transition parameters on $|S_{11}|$ are studied in the following. A parametric analysis is performed on this back-to-back structure and the impact of d_y , d_x , and d_{sc} variation on $|S_{11}|$ is shown, respectively.

Coax position d_{sc}

The effect of the distance from the short circuit to coax on $|S_{11}|$ is shown in Fig. 3.25. To reach a bandwidth that is large enough to cover the filter and DRA integration bandwidth, the $|S_{11}|$ over the bandwidth should ideally be less than $-25 \sim -30$ dB. A suitable value of 2.3 mm is selected, which provides balanced S parameter.

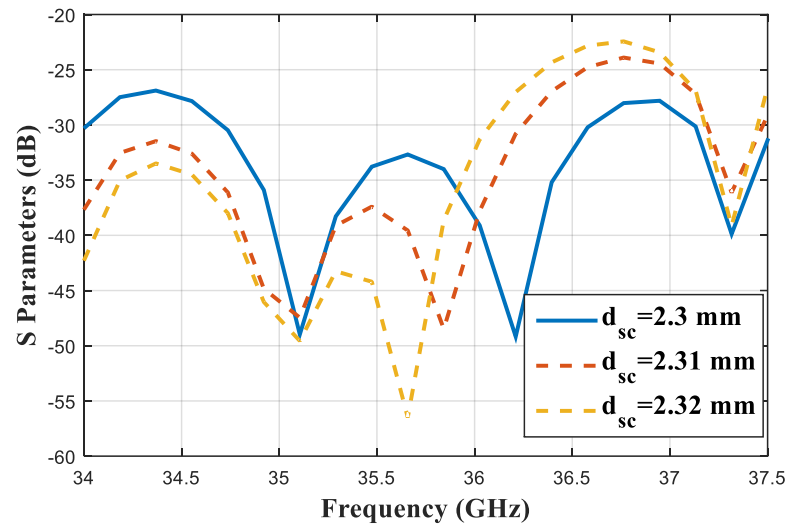


Fig. 3. 25. The impact of coax position d_{sc} variation on $|S_{11}|$ (dB), $d_x=2.18$ mm, and $d_y=3.35$ mm.

Position of matching vias

Two vias are added to match the impedance and the positions of them are studied with results shown in Fig. 3.26 and Fig. 3.27.

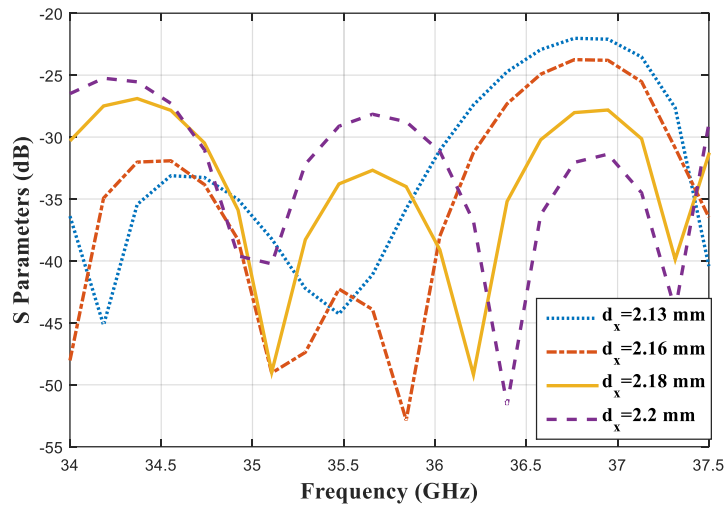


Fig. 3. 26. The impact of tuning screws x-position d_x variation on $|S_{11}|$ (dB).

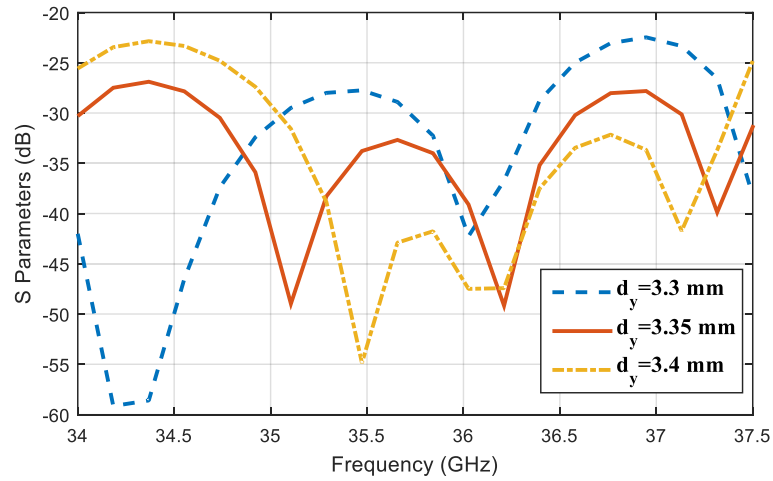


Fig. 3. 27. The impact of tuning screws y-position d_y variation on $|S_{11}|$ (dB).

Parameters are selected to provide low $|S_{11}|$ in the frequency range. The transition with optimized parameters is simulated and the performance is compared to the filter antenna

integration. It is obvious that $|S_{11}|$ of the back-to-back structure is well below -25dB within the bandwidth, as shown in Fig. 3.28.

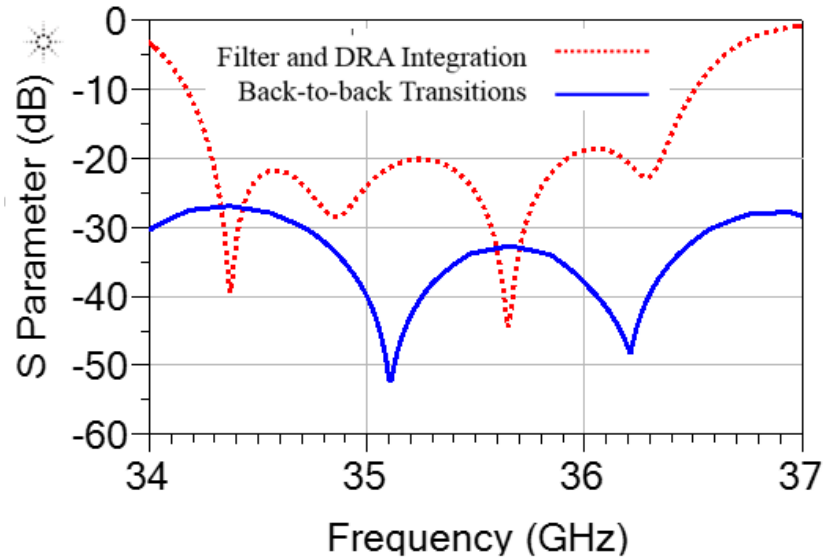


Fig. 3. 28. The simulated $|S_{11}|$ of back-to-back transitions compared with $|S_{11}|$ of filter and antenna integration.

After adding the coax-to-SIW transition, the final configuration of filter antenna integration is shown in Fig.3.29 and Fig.3.30. $|S_{11}|$ and gain as a function of frequency of DRA and filter integration with coax-to-SIW transition are shown in Fig. 3.31. Radiation is shown in Fig. 3.32.

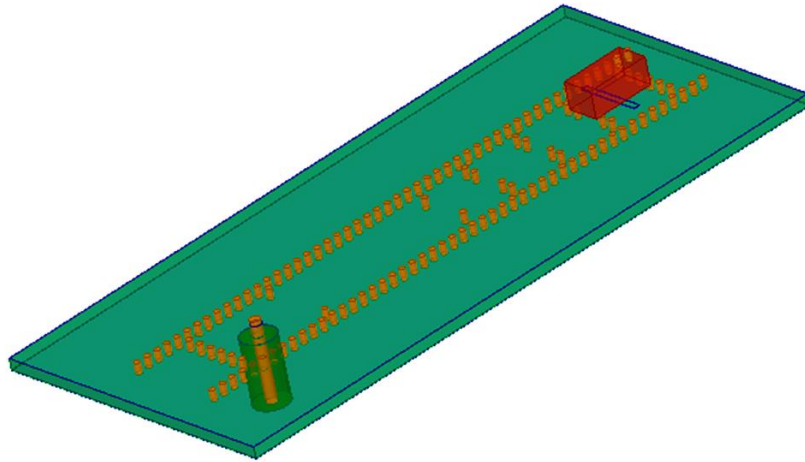


Fig. 3. 29. 3-D model of SIW filter and DRA integration with coax-to-SIW transition.

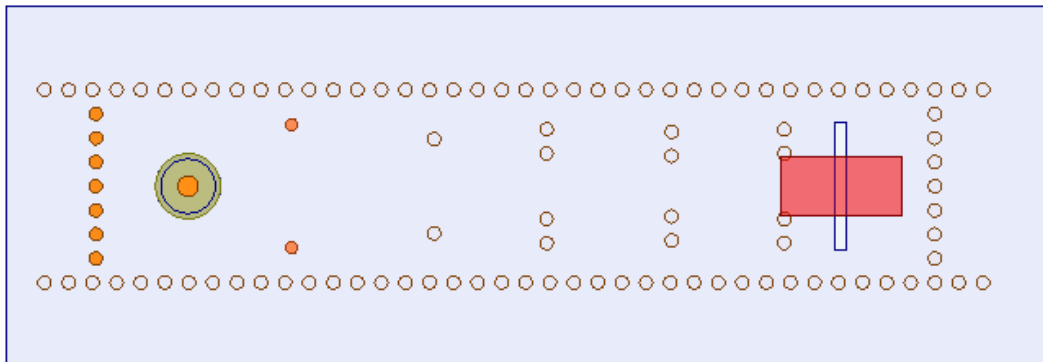


Fig. 3. 30. Top view of SIW filter DRA integration with coax-to-SIW transition.

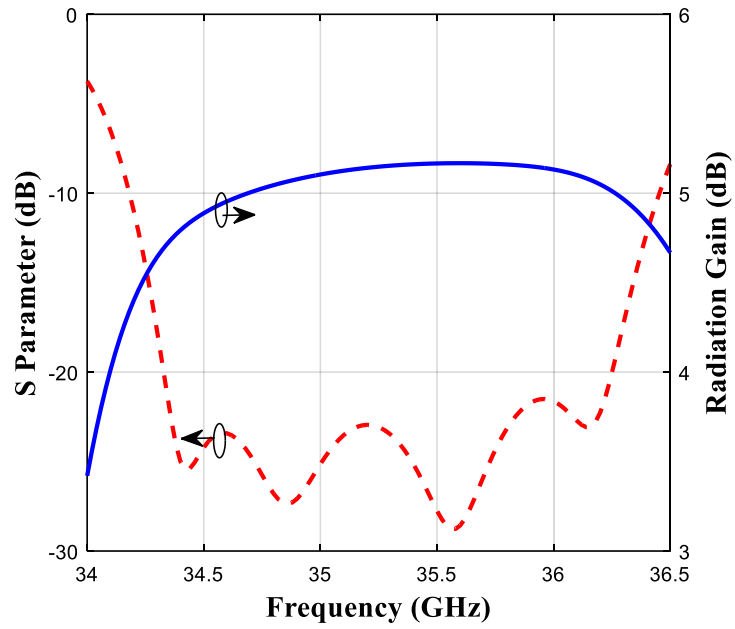


Fig. 3. 31. $|S_{11}|$ and gain of DRA and filter integration.

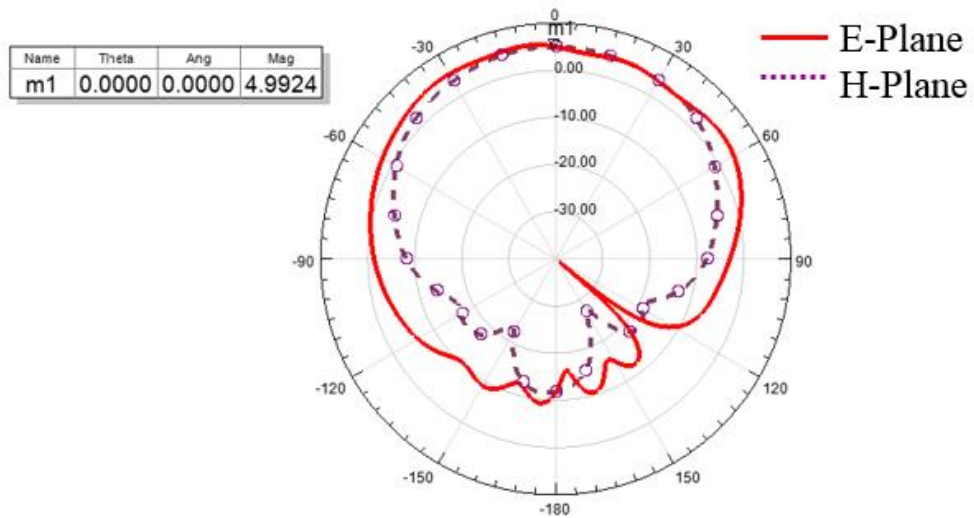


Fig. 3. 32. Radiation pattern of DRA and filter integration.

3.6 Integration of Filter with DRA Array

In this section, DRA array is integrated with SIW filter. The equivalent circuit model is discussed to simplify the optimization of the design. Fig.3.33 shows a 6-element DRA array.

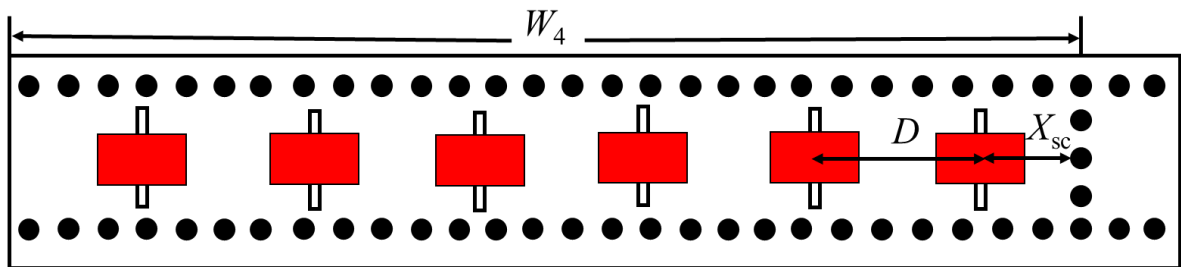


Fig. 3. 33. The schematic of 6-element DRA array

First, we start with a two-element DRA array, to investigate the characteristics of a DRA array. The two-element DRA array is shown in Fig. 3.34. The distance between two elements is defined as D , which is an important design parameter. D affects the phase difference between two elements. As a result, it affects the radiation pattern of the design. This value is initially set to be λ_g . The length from the last element to the short circuit, X_{sc} , affects the input impedance of the antenna array, and it can be analyzed the same way as single DRA.

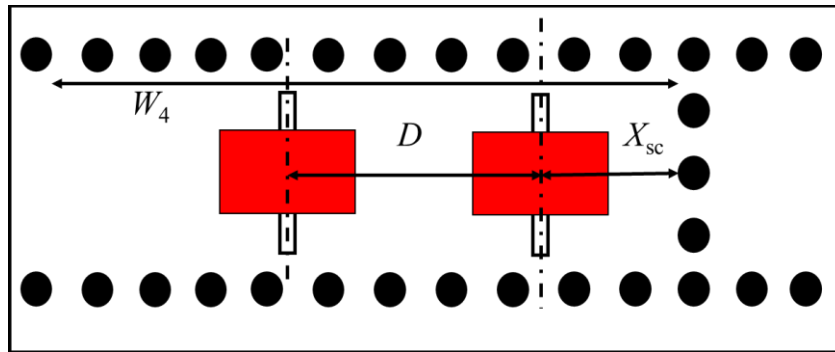


Fig. 3. 34. Design of two-element DRA array.

To get the achievable Q_{ext} of the DRA array, phase of S_{11} and the normalized input impedance of the structure in Fig. 3.34 are shown in Fig. 3.35 and Fig. 3.36. A series RLC equivalent circuit model is compared to the input impedance of DRA array, and it shows that, within the frequency range of interest (34.5 -36.5 GHz), the behavior of DRA array resembles that of a series RLC circuit model, as shown in Fig. 3.36.

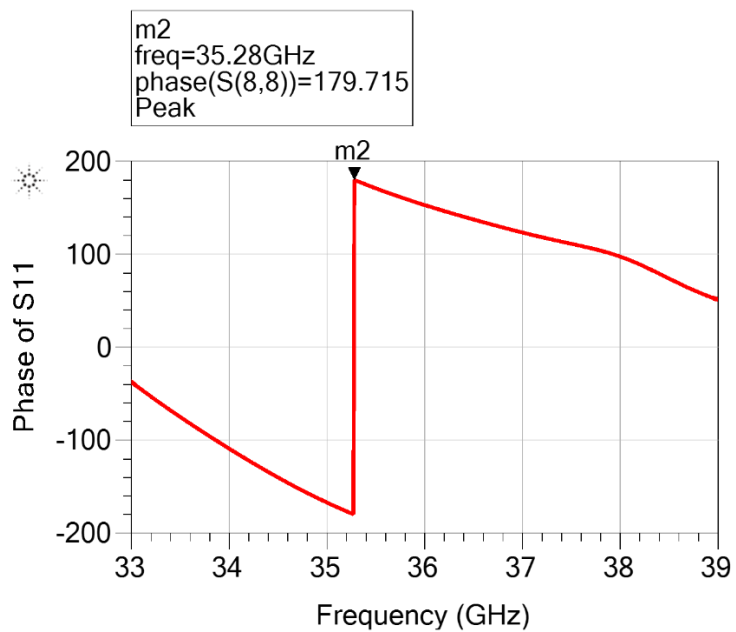


Fig. 3. 35. Phase of S_{11} of DRA array.

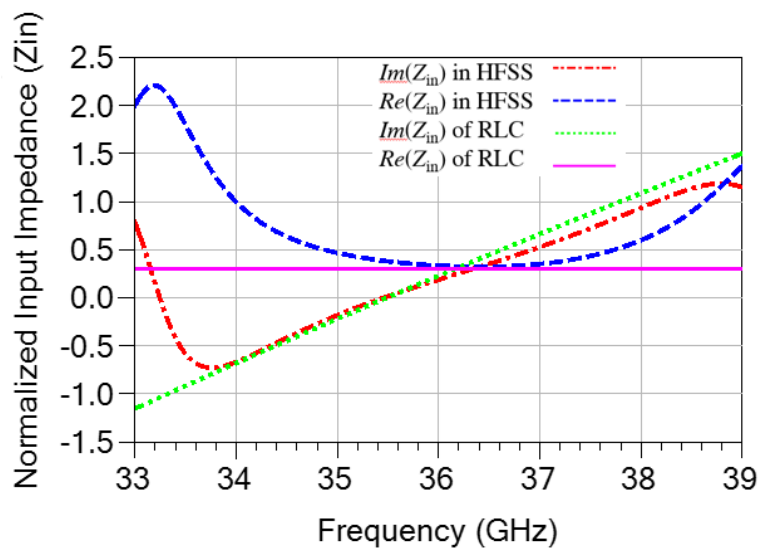


Fig. 3. 36. Normalized input impedance of DRA array in HFSS and its equivalent circuit model in ADS.

Similarly, equation (3.10) and (3.11) can be adopted to calculate the Q_{ext} , and a design curve of Q_{ext} vs. X_{sc} can be derived, which is shown in Fig.3.37. The distance W_4 is adjusted to have the phase of S_{11} as 180° at the center frequency. The achievable range of Q_{ext} is much narrower compared to the Q_{ext} of single DRA.

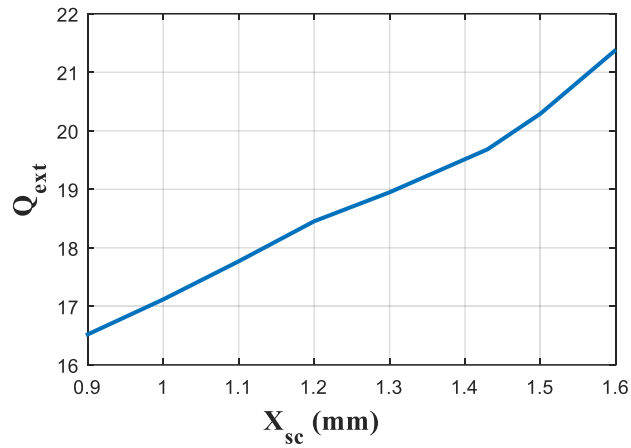


Fig. 3. 37. The design curve of Q_{ext} vs. X_{sc} .

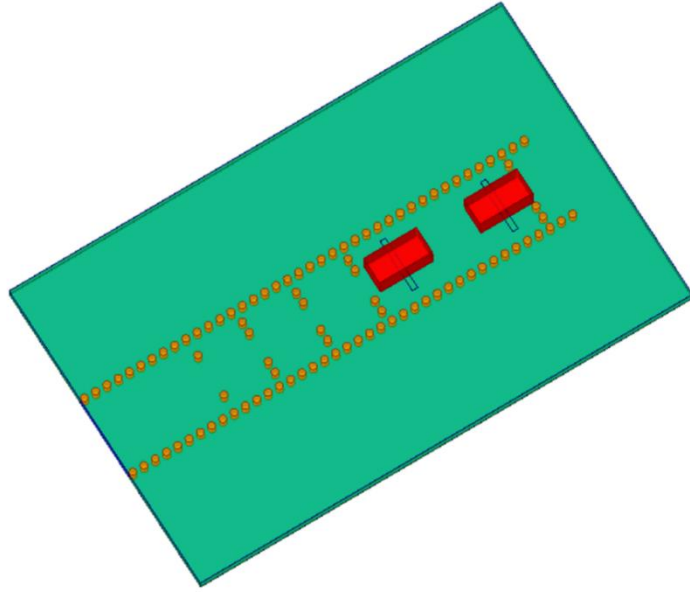


Fig. 3. 38. 3-D model of SIW filter and two-element DRA array integration.

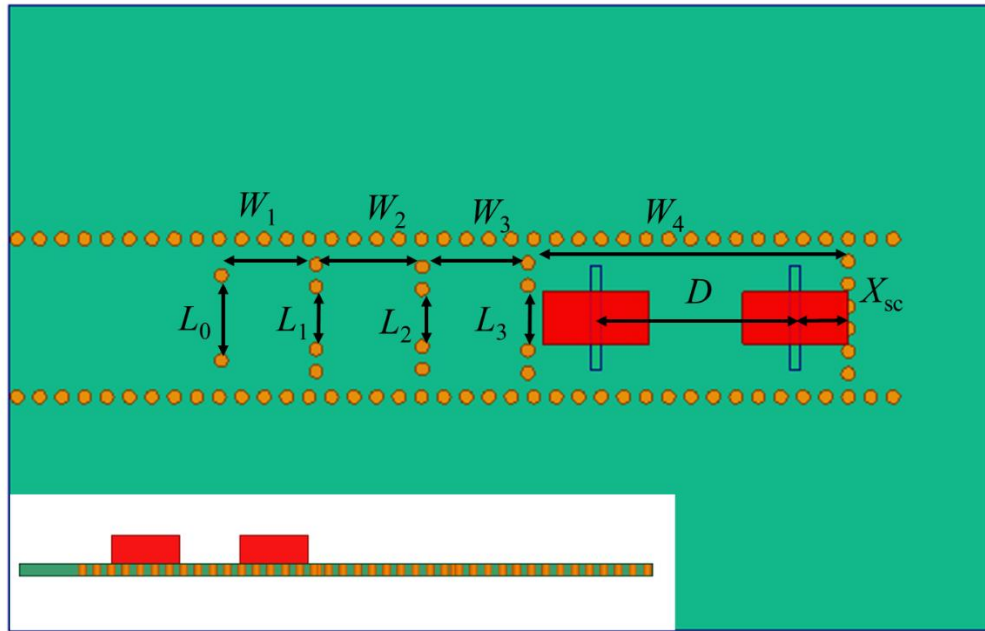


Fig. 3. 39. Top view and side view of SIW filter and two-element DRA array integration
 ($L_0= 2.032$ mm, $L_1=1.384$ mm, $L_2= 1.244$ mm, $L_3= 1.473$ mm, $W_1=2.326$ mm, $W_2= 2.641$
 mm, $W_3= 2.629$ mm, $W_4= 8.75$ mm, $D= 5.7$ mm, $X_{sc}=1.31$ mm)

Then, the DRA array replaces the last resonator and the port of SIW filter, to form the integration. The model is shown in Fig. 3.38, and dimensions are shown in Fig. 3.39.

Also, the parameter extraction is performed on filter and DRA array integration to optimize the parameters. The DRA array with two ports de-embedded to center is imported to ADS, with two transmission lines in front of and behind it. The coarse model and fine model can be optimized to match with each other, as the $|S_{11}|$ shown in Fig. 3.40. The radiation pattern is presented in Fig. 3.41 (a), and the gain is shown in Fig. 3.41 (b), with the achievable radiation gain of 6.99dB.

Based on similar steps, a 6-element DRA array integrated with SIW filter model is given in Fig. 3.42 and 3.43. The simulated $|S_{11}|$ and radiation pattern are given in Fig. 3.44.

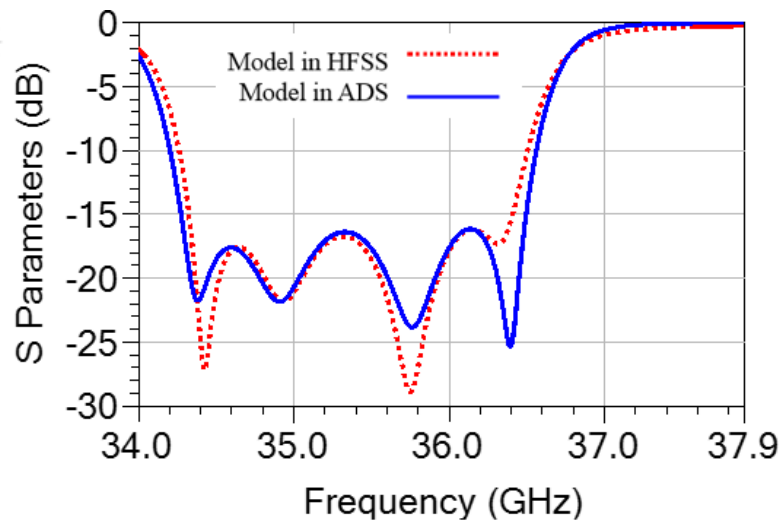
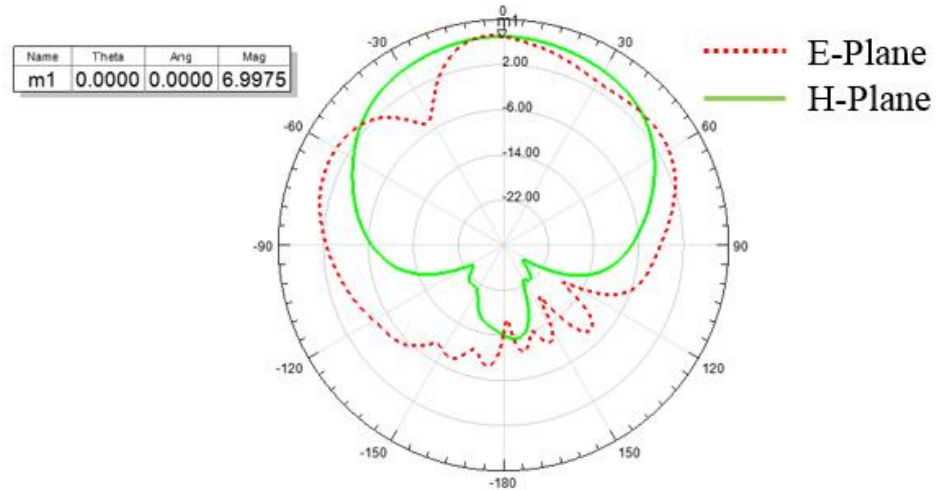
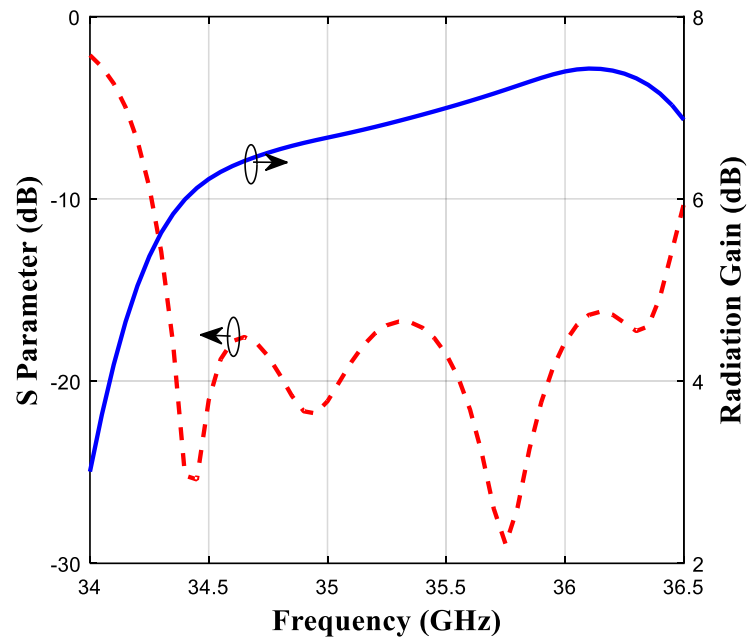


Fig. 3. 40. The match of fine model from HFSS and coarse model in ADS.



(a)



(b)

Fig. 3. 41. (a) Radiation pattern and (b) $|S_{11}|$ and gain of filter with DRA array integration.

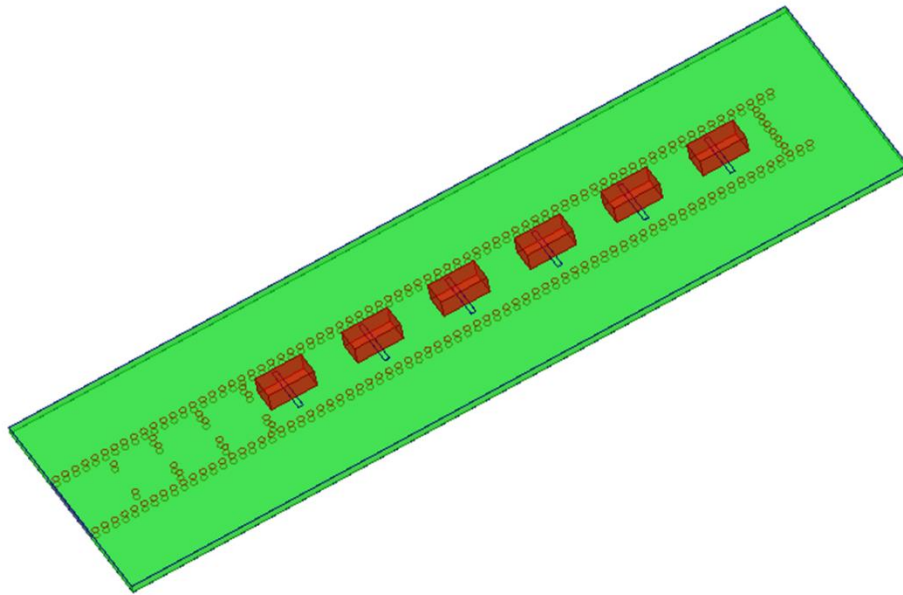


Fig. 3. 42. 3-D model of SIW filter and 6-element DRA array integration.

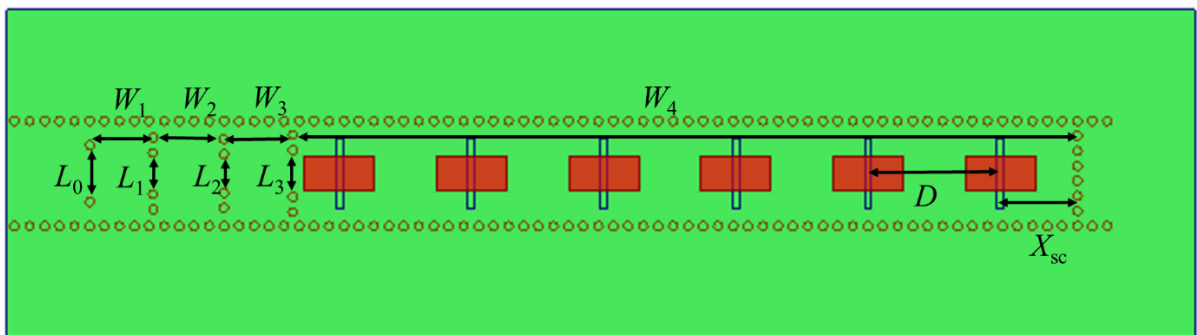
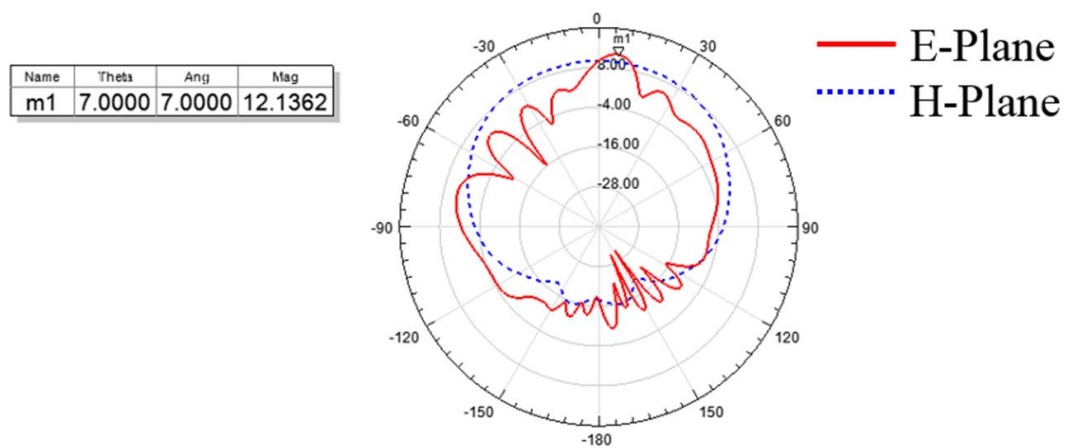
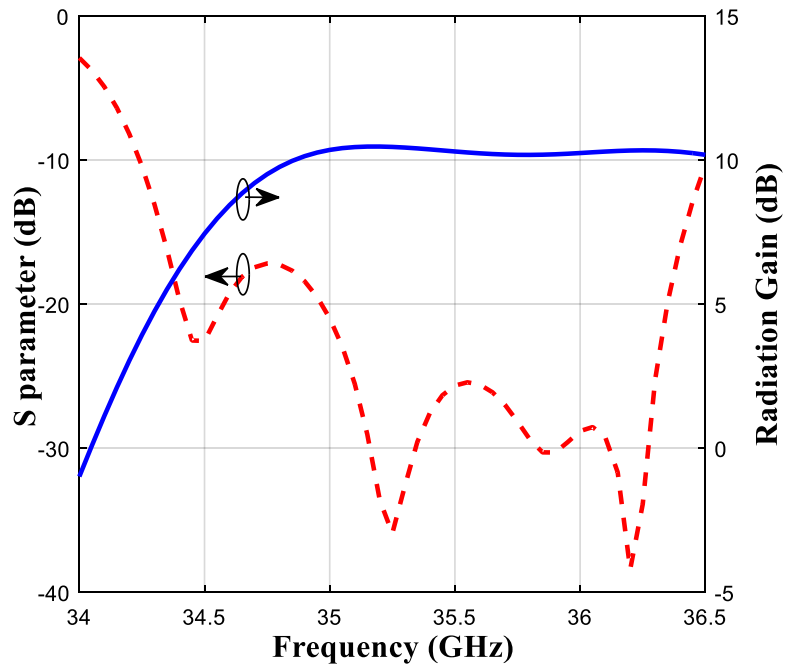


Fig. 3. 43. Top view of the model ($L_0= 2.032$ mm, $L_1=1.384$ mm, $L_2= 1.27$ mm, $L_3= 1.636$ mm, $W_1=2.326$ mm, $W_2= 2.641$ mm, $W_3= 2.57$ mm, $W_4= 33.36$ mm, $D= 5.65$ mm, $X_{sc}=2.31$ mm).



(a)



(b)

Fig. 3. 44. (a) Radiation pattern and (b) gain of the model and $|S_{11}|$ of SIW filter and 6-element DRA array integration model.

3.7 Integration of Filter with Parasitic DRA

In the antenna array design, a lot of methods are involved to increase the radiation gain and bandwidth of antenna, which are the most important properties for an antenna. For microstrip antennas, it has been proven that, by adding parasitic elements to the driven antenna, the radiation gain can be greatly increased, the radiation can be steered and the bandwidth can be increased [63, 64]. Different from antenna array, the parasitic antennas only have one excitation to the driven antenna, and the parasitic elements are simply mounted around the driven antenna at certain distance. Similar to the microstrip antenna, the radiation gain of DRA can also be increased by adding parasitic elements [65].

Fig. 3.45 shows the parasitic DRA structure. Two parasitic elements are added symmetrically to both sides of the driven DRA, and the distance D between them is initially set to be half of the wavelength.

The filter integration with parasitic DRA model is give in Fig. 3.46. The simulated $|S_{11}|$ and radiation pattern are shown in Fig. 3.47.

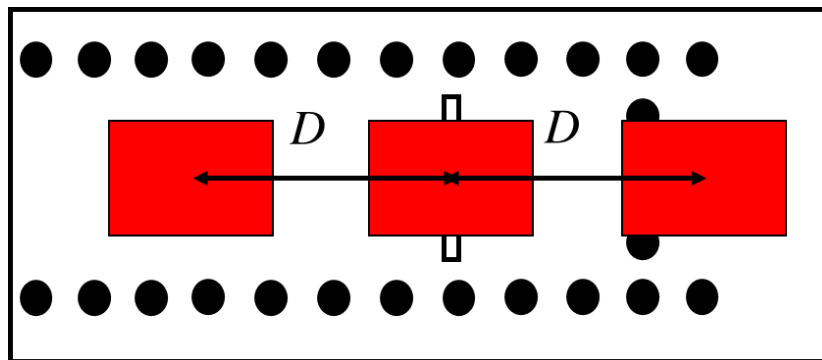


Fig. 3. 45. The parasitic DRA.

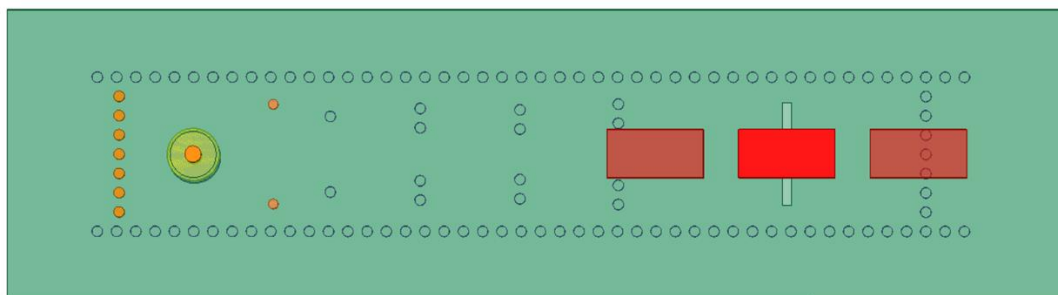
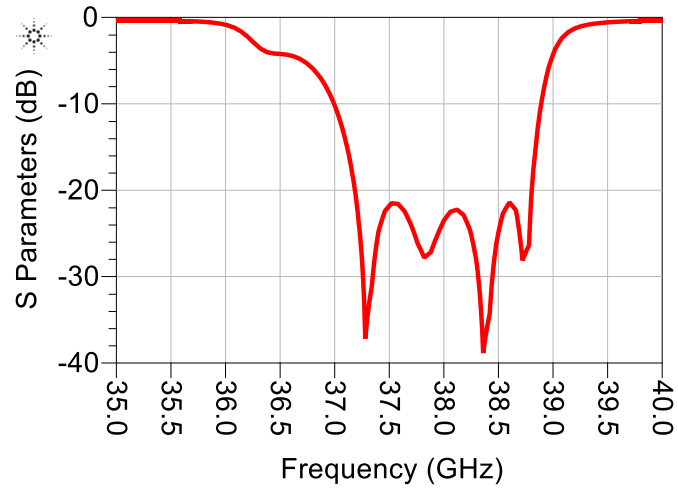
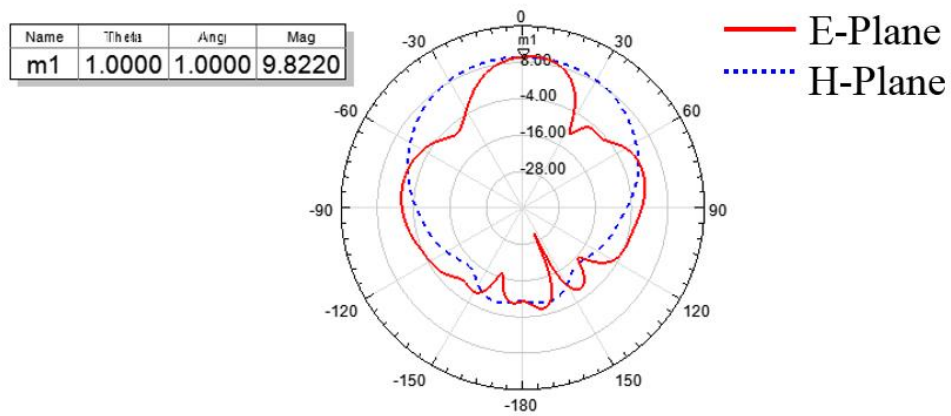


Fig. 3. 46. SIW filter and parasitic DRA integration.



(a)



(b)

Fig. 3. 47. (a) $|S_{11}|$ of SIW filter and parasitic DRA integration, and (b) the radiation pattern of filter and parasitic DRA integration.

3.8 Measurement Results

In this sections, the measurement results of SIW-based DRA, SIW filter with single DRA integration, and SIW filter with parasitic DRA integration are presented. The simulation results and measurement results are compared. The fabricated designs follow the same design synthesis presented in this thesis, but with a center frequency at 37.5 GHz. The material used is *RT/Duroid 6002*, with dielectric constant $\epsilon_r=2.94$. This value is measured at 10GHz frequency and under the environment of 23°C. However, the center frequencies of out designs are 35 GHz and 37.5 GHz, which are much higher than measurement frequency. As a result, the value of dielectric constant ϵ_r varies and leads to shifts in measurement results. Due to fabrication tolerances and varied ϵ_r , there is mismatch between measurement and simulation results. So a tolerance analysis is performed and presented in this section.

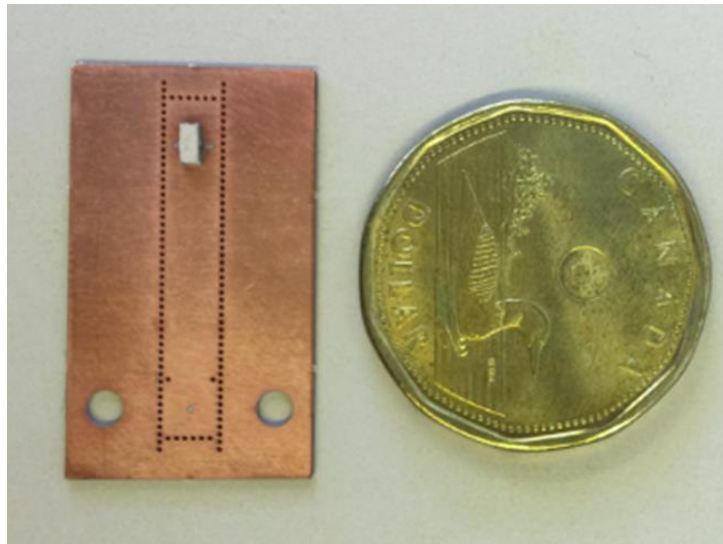


Fig. 3. 48. Photograph of SIW-based DRA structure.

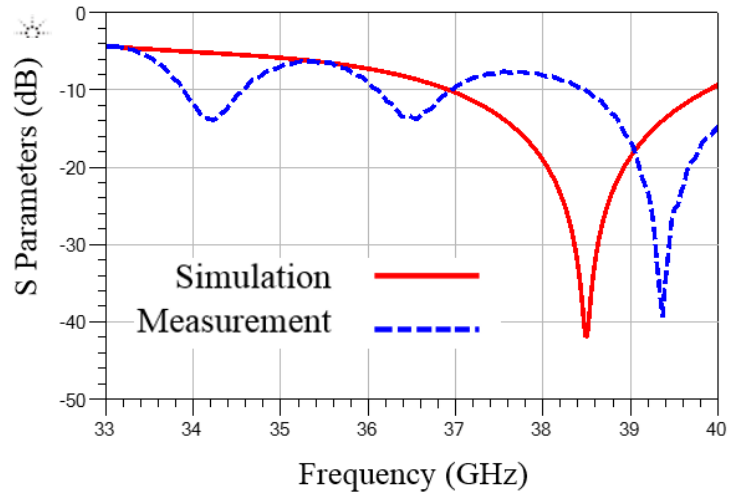


Fig. 3. 49. $|S_{11}|$ of simulation and measurement for SIW-based DRA model.

A picture of the SIW-fed DRA is shown in Fig. 3.48 and the measurement results are shown in Fig. 3.49 to compare with simulation results. Misalignment is observed between simulation and measurement results. This is mainly caused by inaccuracy of the material dielectric constant and fabrication tolerances. The width of SIW, a_{SIW} , has larger impact on center frequency among all design parameters. Therefore, in the following tolerance analysis, the dielectric constant ϵ_r and SIW width, a_{SIW} , are studied.

First, the dielectric constant is varied and simulations using different dielectric constant for the substrate are analysed to match the frequency response from measurement. Fig. 3.50 shows that when $\epsilon_r=2.87$, there is a good agreement between measurement and simulation.

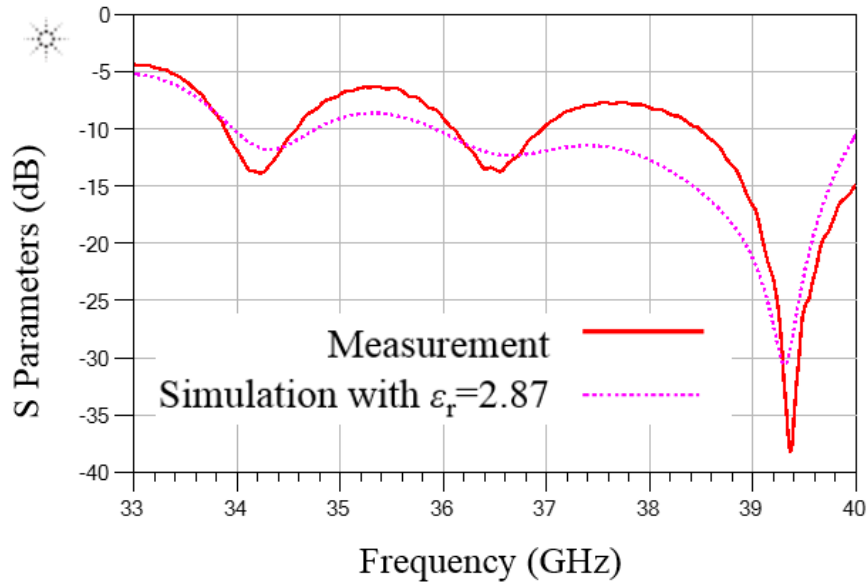


Fig. 3. 50. $|S_{11}|$ of measurement and simulation with $\epsilon_r=2.87$.

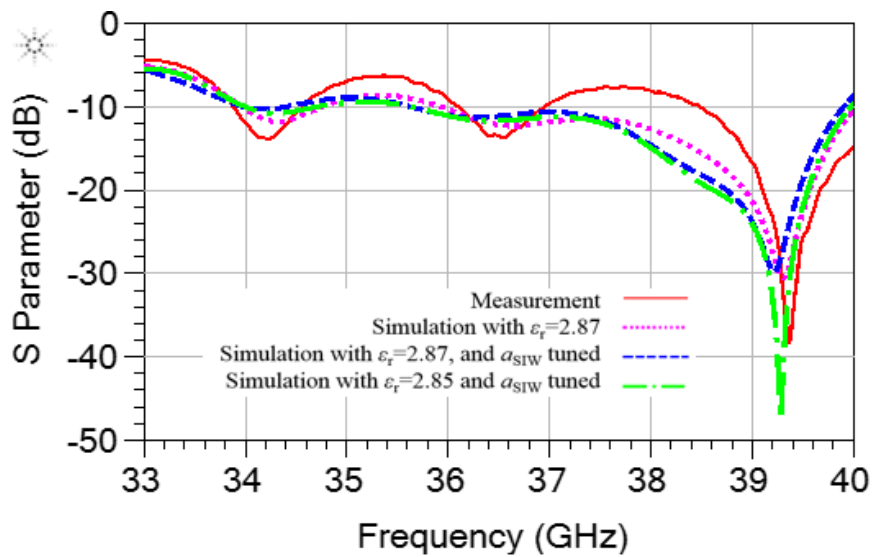


Fig. 3. 51. $|S_{11}|$ of measurement and simulation results.

The SIW width a_{SIW} is also studied to account for tolerances. As indicated in short dashed line in Fig. 3.51, when the width is changed, the peak shifts to lower frequency. As a result, the dielectric constant needs to be smaller, the center frequency would shift to higher value.

The long dashed line in Fig. 3.51 indicates that with newly tuned a_{SIW} and $\epsilon_r=2.85$, the center frequencies of measured and simulated results are closer to each other.

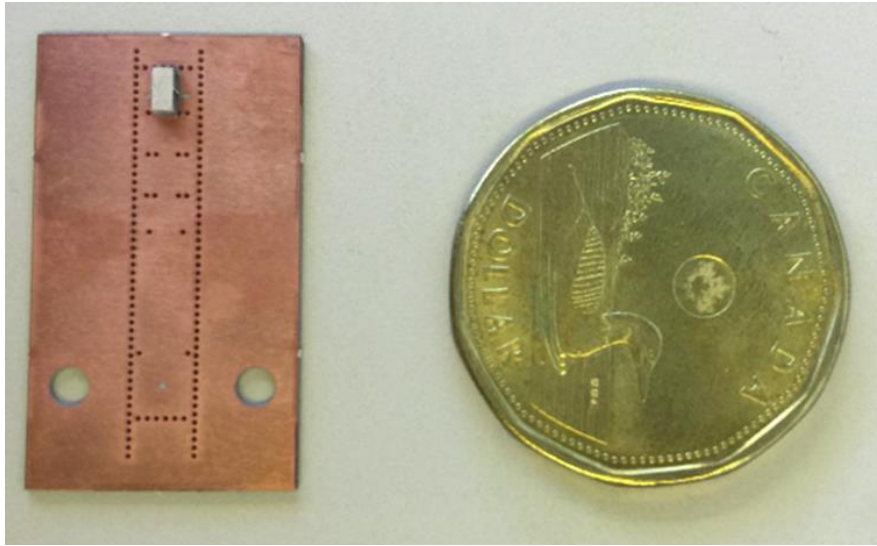


Fig. 3. 52. Photograph of SIW filter with DRA integration.

With the new dimensions, the SIW filter with single DRA is also studied. A picture of the fabricated SIW filter with DRA integration is shown in Fig. 3.52. First, the simulation and measured results are shown in Fig. 3.53. It shows that the frequency shifts up about 1 GHz. Bandwidth of simulated model is 1.72 GHz, while the measured bandwidth is 1.66 GHz. Next, the tolerance analysis is performed on the model. With newly tuned a_{SIW} and $\epsilon_r=2.85$, the center frequencies get closer to each other, as shown in Fig. 3.54.

Fig. 3.55 shows a photograph of the integrated design of the SIW filter with parasitic DRA. The measurement results are compared with simulation in Fig. 3.56, showing a similar shift in the center frequency. Also, a tolerance analysis is operated on this model. With $\epsilon_r=2.85$

and some minor changes to dimensions to account for tolerances, the S_{11} parameters have better alignment. It proves that the shifts in center frequency are mainly caused by fabrication tolerance and inaccuracy of dielectric constant ϵ_r .

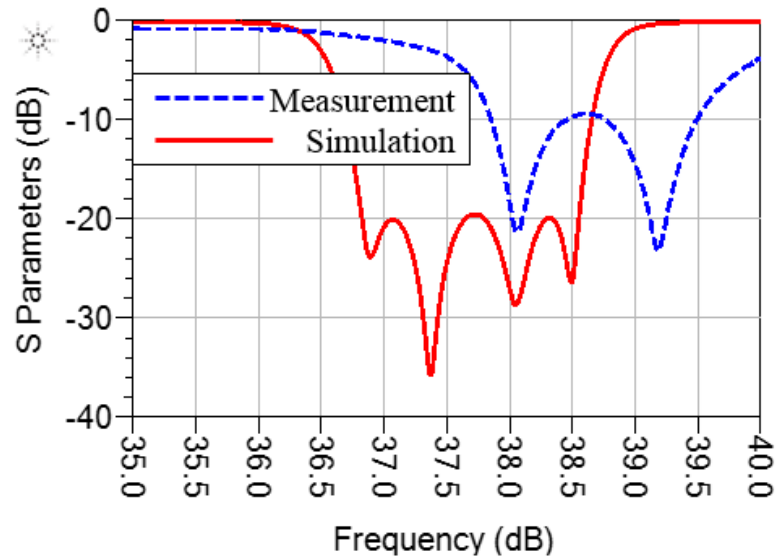


Fig. 3. 53. Simulation and measurement results for filter with single DRA integration.

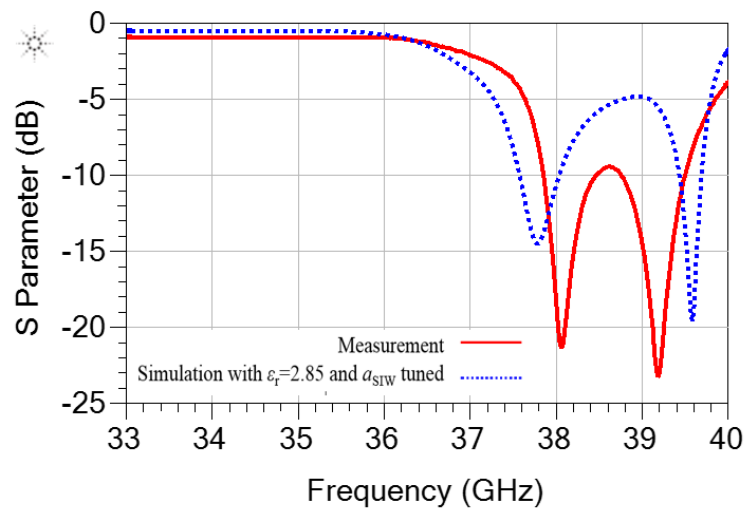


Fig. 3. 54. Tolerance analysis for filter with single DRA integration and measurement results.

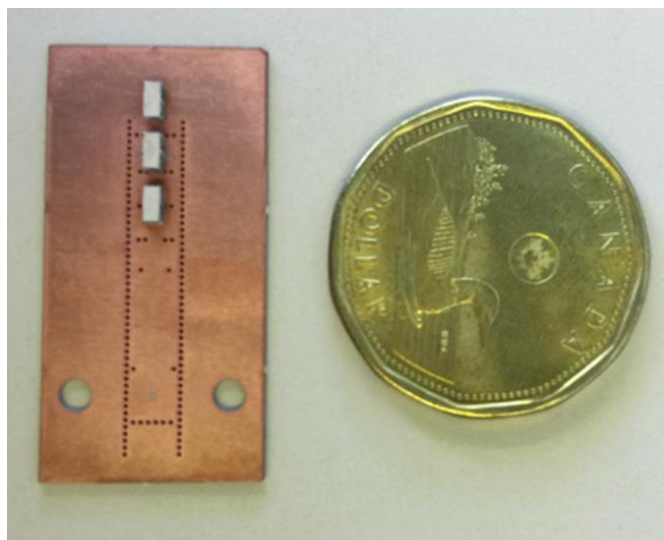


Fig. 3. 55. Photograph of SIW filter with parasitic DRA integration.

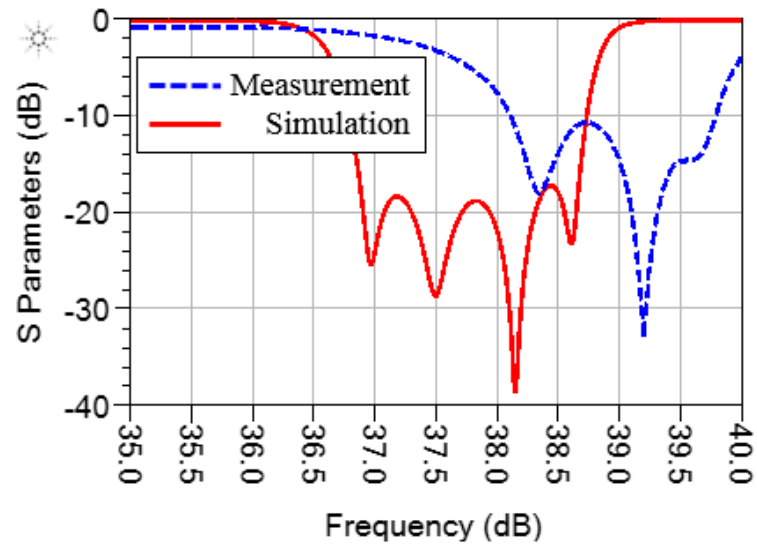


Fig. 3. 56. Simulation and measurement results for filter with parasitic DRA integration.

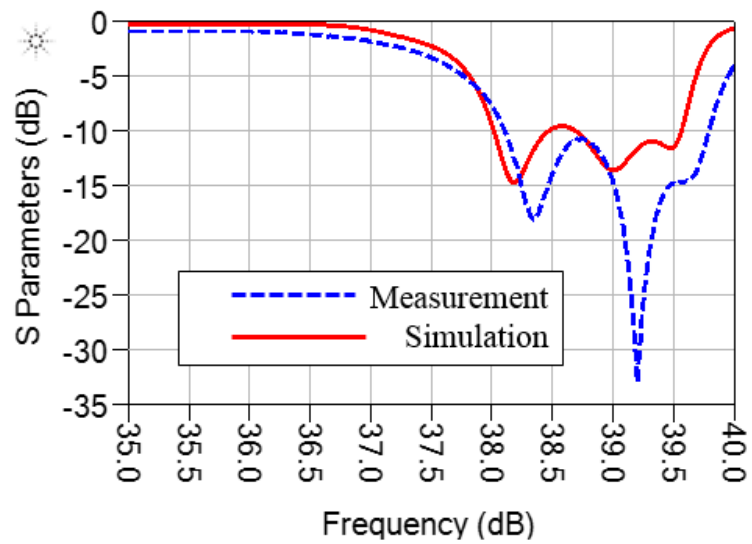


Fig. 3. 57. Tolerance analysis for filter with parasitic DRA integration and measurement results.

3.9 Summary

This chapter gives details on the synthesis procedure of SIW filter and DRA integration. First, a SIW filter is designed at the center frequency, with return loss less than -20dB. Then, a DRA based on SIW is designed to have the same resonant frequency. An integration is implemented by directly connecting DRA to the third cavity of the filter. Replacing the last resonator and the load, the DRA works as a resonator cavity for the filter, and the radiator at the same time. Similar procedures are applied to integration with DRA array and parasitic DRA. Design examples are given. Simulations and measurements are presented.

CHAPTER 4

Integration of Microstrip Bandpass Filter with Inset-Fed Patch Antenna

In this chapter, the integration of microstrip patch antenna with filter is studied for the improvement of coupling values. A direct connection method is used as the coupling method between an inset-fed patch antenna and the filter. Comparison is made with the proximity coupling method reported in the literature [66]. The proximity coupling is realized by the gap between a rectangular patch antenna and the last resonator filter of a hairpin filter. It is difficult to realize strong coupling, since the gap becomes very small.

The proximity coupling method is therefore not compatible with wideband designs [67-70].

It will be shown that a much larger range of coupling coefficient can be readily achieved for the coupling method with the direct connection. As a result, a wider achievable bandwidth can be realized. A design example is given and the simulation results are presented in this chapter.

4.1 Design of the Filter

For demonstration and comparison, a conventional hairpin bandpass filter is used. The parallel-couples, half-wavelength resonator is folded into “U” shape to save space, and filters built by this “U” shape resonator are called hairpin filters. The fractional bandwidth is 4.1% and the center frequency is 2.2 GHz. A three-pole Chebyshev lowpass prototype is chosen with equal ripple $L_{ar}=0.1$ dB. The prototype parameters are normalized to lowpass cut off frequency $\Omega_c=1$ and listed below:

$$g_0 = g_4 = 1, g_1 = g_3 = 1.0316, g_2 = 1.1474$$

The bandpass design parameters can be derived from the prototype parameters as:

$$Q_{ext} = \frac{g_0 g_1}{FBW} = \frac{g_4 g_5}{FBW} \quad (4.1)$$

$$k_{ij} = \frac{FBW}{\sqrt{g_i g_j}}, \quad (4.2)$$

Q_{ext} is the external Q -factor, and k_{ij} is the inter-resonator coupling between adjacent resonators. So the design parameters are: $Q_{ext} = 25.16, k_{12} = k_{23} = 0.0377$.

The width of the hairpin resonator arm is 1 mm, and the distance between two hairpin arms is 8.1 mm. If this distance is too small, the coupling between two arms will affect the couplings. A 2.04 mm-thick substrate with $\epsilon_r = 4.1$ and $\tan\delta = 0.0035$ is used. The design of hairpin bandpass filter is shown in Fig. 4.1.

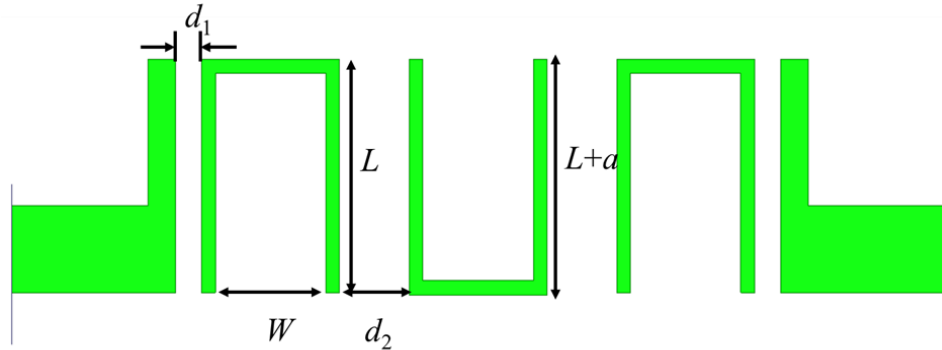


Fig. 4. 1. Three-pole hairpin bandpass filter ($W=8.1$ mm, $d_1=1.63$ mm, $d_2=5.11$ mm, $L=16.34$ mm, and $a=0.2$ mm).

First, Ansoft High Frequency Structure Simulator (HFSS) is used to extract design parameters. External Q -factor is the coupling between the first resonator to the load. A model is built to extract Q_{ext} . Another side of hairpin resonator is weakly coupled to the port. And the External Q -factor is easily obtained from HFSS solutions using equation (4.3) [12]:

$$Q_{ext} = \frac{f_0}{(\Delta f)_{3dB}} \quad (4.3)$$

where $(\Delta f)_{3dB}$ is the 3dB bandwidth. The design curve of Q_{ext} vs. distance d_1 is given in Fig. 4.2.

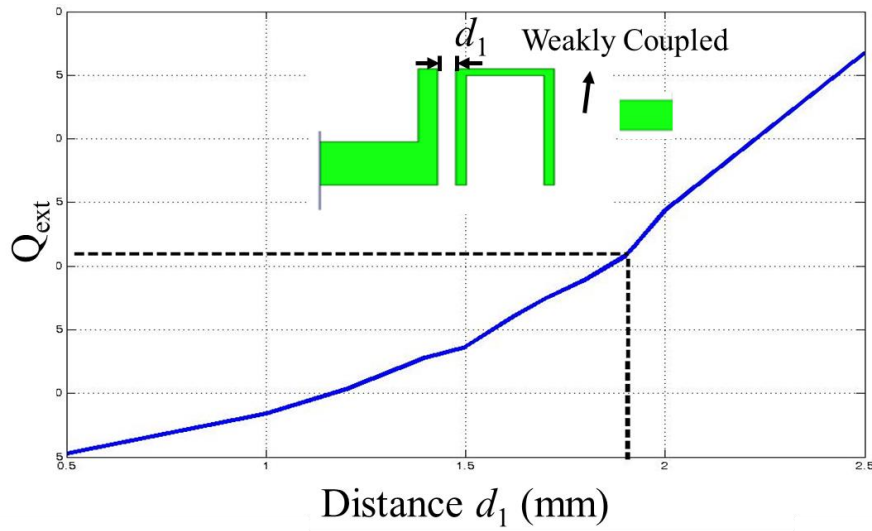


Fig. 4. 2. Design curve of Q_{ext} as a function of distance d_1 , and the simulation model.

Then, two hairpin resonators are built in HFSS and Eigenmode solver in HFSS is used with mode number set as 2. After the simulation, two resonant frequencies are obtained and used to calculate the inter-resonator coupling coefficient k_{ij} through [12]:

$$k_{ij} = \frac{f_2^2 - f_1^2}{f_2^2 + f_1^2} \quad (4.3)$$

A design curve of k_{ij} as a function of distance d_2 can be derived from the simulations, as plotted in Fig. 4.3.

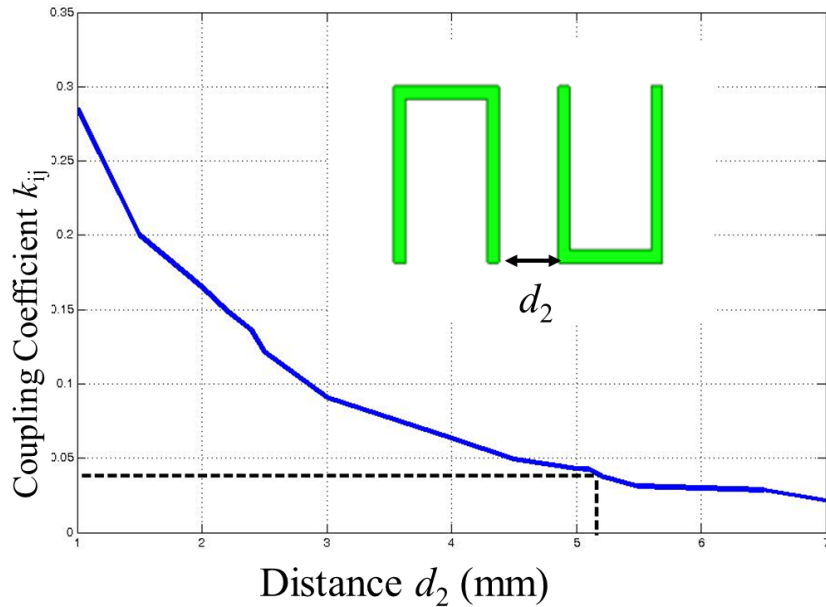


Fig. 4. 3. Design curve of coupling coefficient k_{ij} as a function of distance d_2 , and the simulation model.

4.2 Design of the Inset-Fed Microstrip Patch Antenna

Microstrip patch antenna is widely used in RF/microwave applications due to its low-profile, light weight, ease of fabrication, and low cost. It consists of a copper patch, a substrate filled with dielectric material, and feeding mechanism. The copper patch can be different shapes. Square, rectangular, circular, thick strip and elliptical are mostly used. Also, a number of feeding methods can be used to excite microstrip patch antenna, such as coaxial probe [71], [72], microstrip line [73], proximity coupling [74], etc. Fig. 4.4 shows a rectangular patch antenna with inset-fed model. Inset-fed is one of the microstrip line feeding mechanisms. At the side of patch antenna, the input

impedance reaches the maximum value, and gradually reduces to zero at center. So the inset depth y_0 can change the input impedance of antenna.

The design rule of a rectangular patch antenna concerns the center frequency, and dielectric constant ϵ_r of the substrate material. The width and length of patch antenna can be calculated using [75]:

$$W_p = \frac{c}{2f_0 \sqrt{\frac{\epsilon_r + 1}{2}}} \quad (4.3)$$

$$L_p = \frac{c}{2f_0 \sqrt{\epsilon_{eff}}} - 2\Delta L \quad (4.4)$$

where

$$\epsilon_{eff} = \frac{\epsilon_r + 1}{2} + \frac{\epsilon_r - 1}{2 \sqrt{1 + 12 \frac{h}{W_p}}} \quad (4.5)$$

$$\Delta L = 0.412h \frac{(\epsilon_{eff} + 0.3) \left(\frac{W_p}{h} + 0.264\right)}{(\epsilon_{eff} - 0.258) \left(\frac{W_p}{h} + 0.8\right)} \quad (4.6)$$

The feeding microstrip line has the same dimension as the two gaps beside it, and together they form the inset width D . the inset depth y_0 varies the input impedance as:

$$Z_{in}(y = y_0) = Z_{in}(y = 0) \cos^2\left(\frac{\pi}{L_p} y_0\right) \quad (4.7)$$

where $Z_{in}(y = 0)$ is the input impedance at edge of the patch antenna. With the parameters, a rectangular patch antenna can be built using HFSS. The model is shown in Fig. 4.4 and Fig. 4.5. The substrate is the same as the hairpin filter substrate, and a lumped port is set as the excitation port.

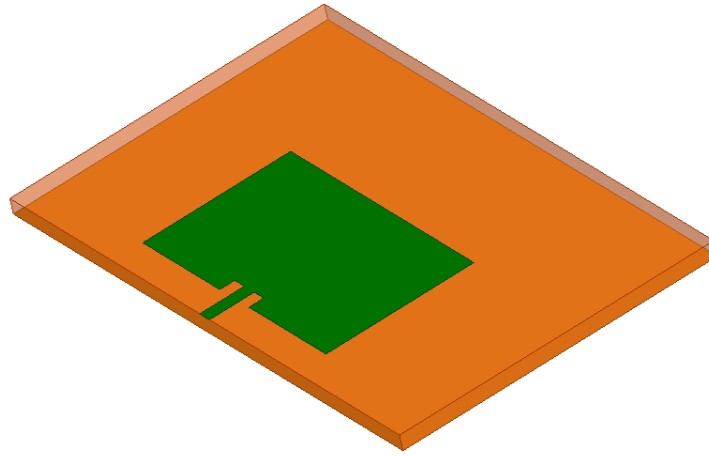


Fig. 4. 4. 3-D model of inset-fed rectangular patch antenna.

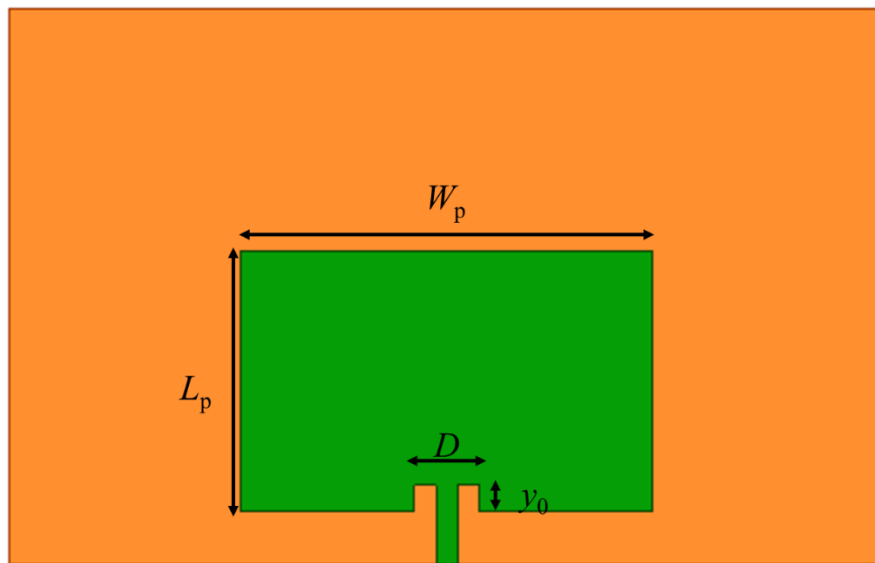


Fig. 4. 5. Top view of antenna model ($L_p=47$ mm, $W_p= 36$ mm, $D= 5$ mm, and $y_0=4.5$ mm)

The simulated $|S_{11}|$ is shown in Fig. 4.6. And the radiation pattern of E-plane and H-plane is given in Fig. 4.7.

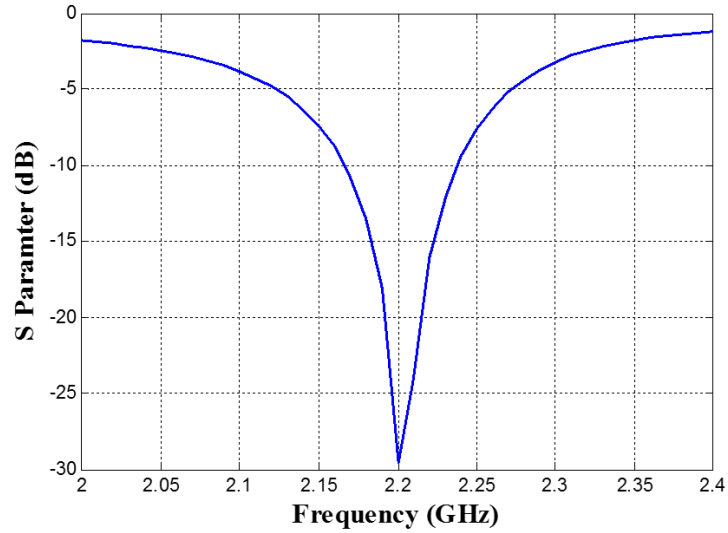


Fig. 4. 6. EM simulated $|S_{11}|$ of inset-fed rectangular patch antenna.

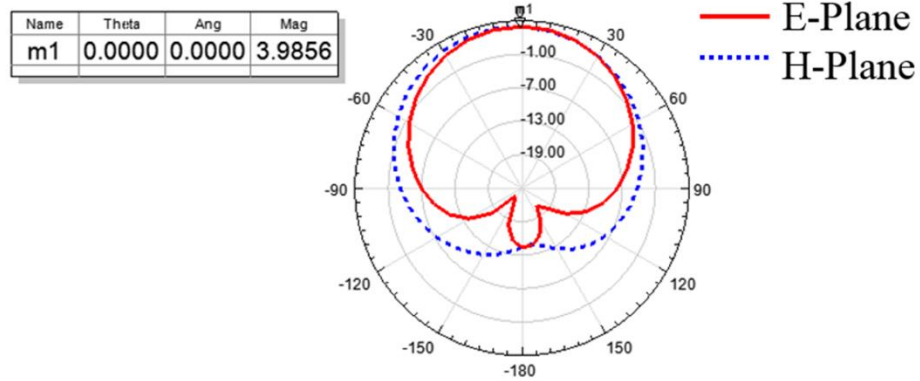


Fig. 4. 7. Radiation pattern of inset-fed rectangular patch antenna.

4.3 The Integration of the Inset-Fed Antenna and Filter

Inset-fed microstrip antennas are commonly used due to many advantages [76]. For improvement of coupling, the antenna feed line is directly connected to the last hairpin resonator, as shown in Fig. 4.8. The inset width D varies the center frequency [77]. To make sure that the rectangular patch antenna resonates at the given center frequency, D should be kept constant. The coupling coefficient between the resonator and the antenna is mainly controlled by changing the distances x_0 and y_0 .

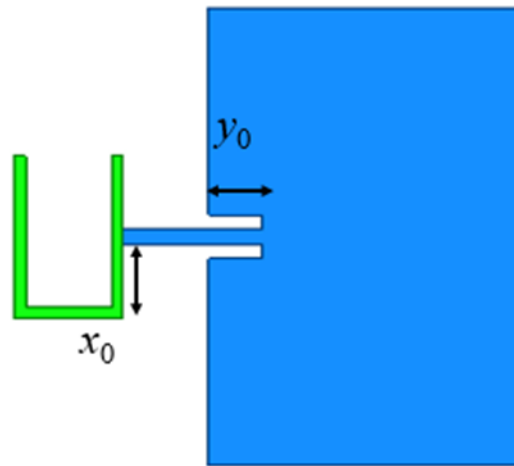


Fig. 4. 8. The direct connection coupling method between the filter resonator and the antenna.

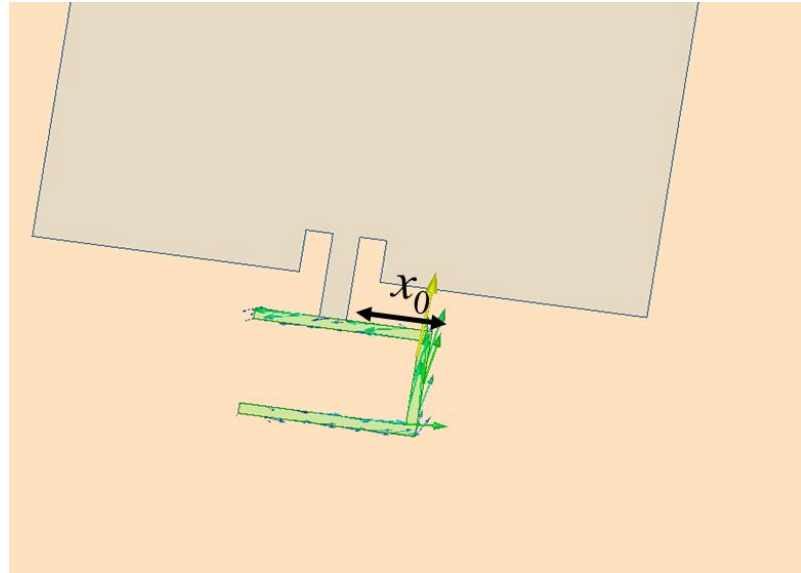


Fig. 4. 9. The circuit flow on the resonator when coupled to the antenna.

Fig. 4.9 shows the current flow on the resonator. The “U” shaped resonator has the minimum current at the open circuit end, while the opposite side has the maximum current. Hence, the coupling coefficient between the resonator and antenna can be controlled via the connection position on the resonator, x_0 . To be more specific, the closer the tap point is to the open circuit end, the smaller the coupling coefficient is. Similarly, the coupling coefficient can be controlled by changing the inset depth, y_0 .

Note that to correctly calculate the coupling coefficient k , the inset-fed patch antenna and the hairpin resonator are first tuned separately to resonate at the same frequency. Eigen mode solver in HFSS is employed to find the resonant frequencies. Both the resonator and

the antenna are slightly adjusted to account for loading effects. Next, the configuration in Fig. 4.8 is simulated to get the coupling coefficient.

For comparison, the proximity coupling [66], shown in Fig. 4.10, is also simulated. Here we use y_0 to denote the distance between the resonator and the patch antenna, which controls the coupling coefficient.

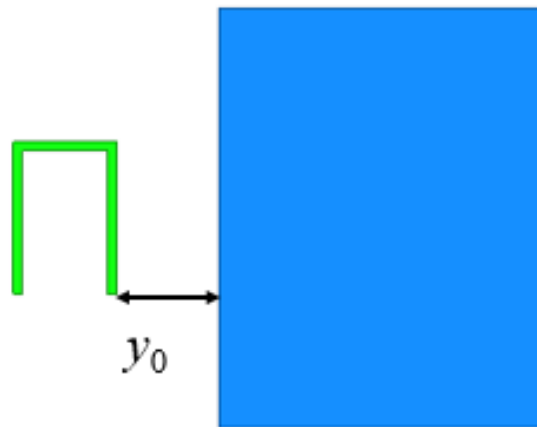


Fig. 4. 10. The proximity coupling method between the filter resonator and the antenna [66].

Fig. 4.11 compares the coupling coefficients realized using proximity and direct connection coupling methods as the distance y_0 varies. Note that y_0 in the two configurations has different meanings, but controls the coupling coefficient in both cases. It can be clearly seen that, compared with the curve for proximity coupling, which is similar to Fig. 7(c) in [66], a much wider range of coupling coefficient is achieved using the direct coupling method. For proximity coupling, if a wider bandwidth design is required, the gap y_0 in Fig.

4.10 needs to be very small, which becomes difficult to fabricate. However the direct coupled method, as shown in Fig. 4.11, can easily realize much larger coupling value.

The configuration of filter antenna integration is shown in Fig. 4.12.

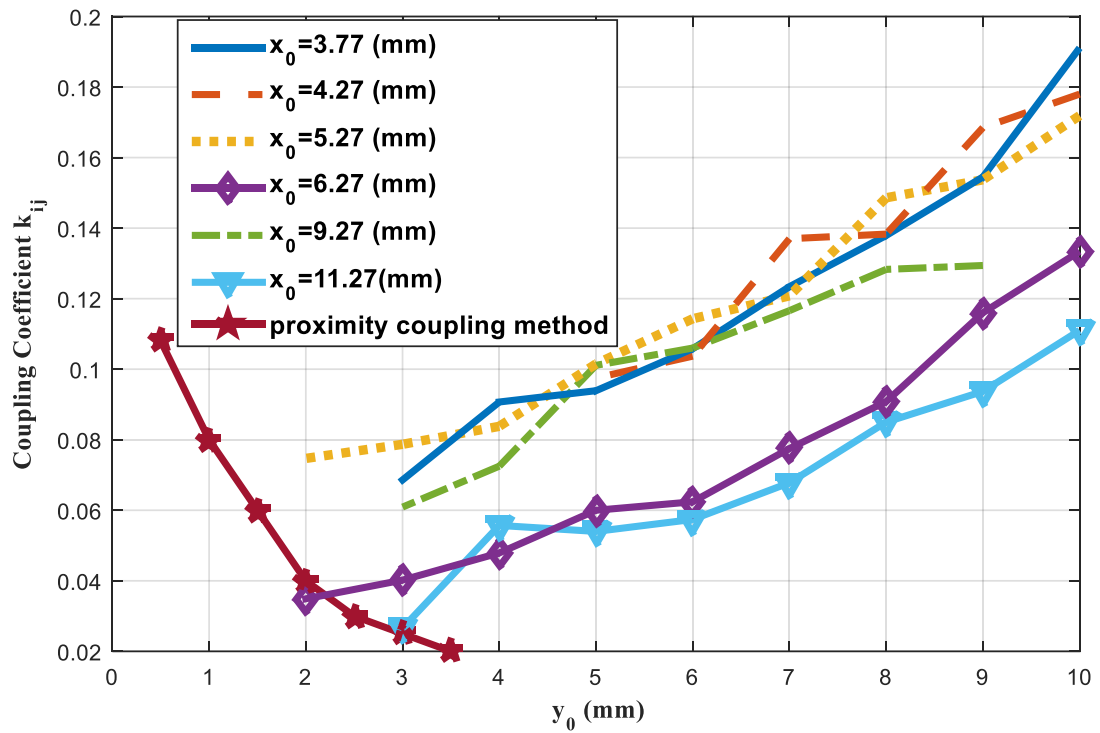


Fig. 4. 11. Comparison of the coupling coefficients realized using proximity and direct connection coupling methods.

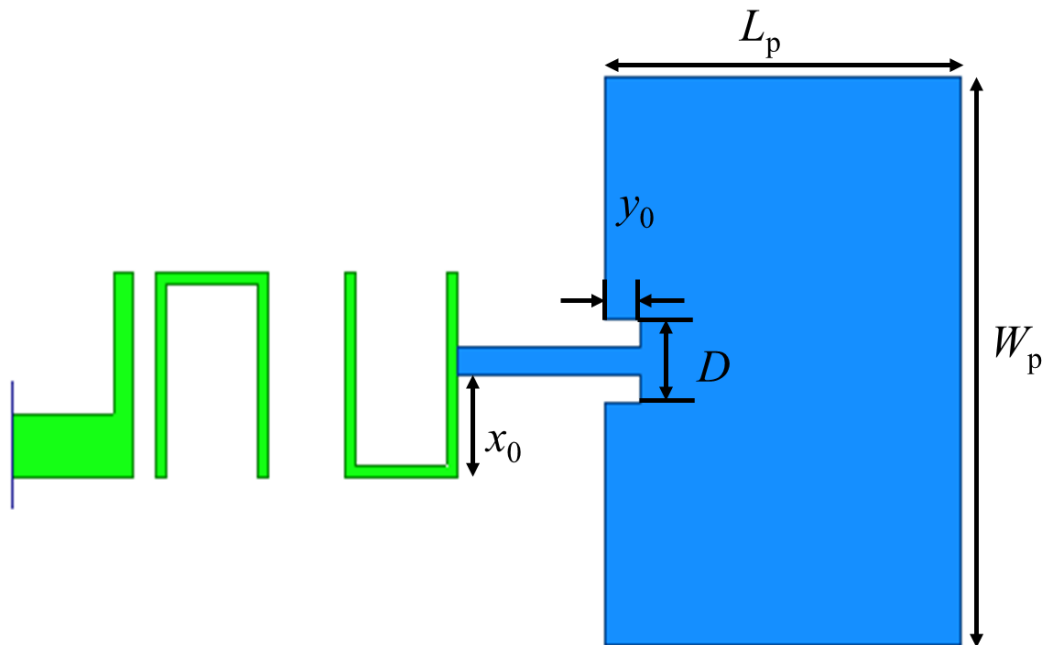


Fig. 4. 12. An example of filter antenna integration ($x_0=6.2$ mm, $L_p=47$ mm, $W_p= 36$ mm, $D= 5$ mm, and $y_0=4.5$ mm).

4.4 Design Example and Simulation Results

Dimensions are given in Fig. 4.12 for the design example. x_0 and y_0 are adjusted so that the coupling coefficient has the same value as k_{23} of the 3-pole filter in Fig. 4.1. The length of the last resonator is tuned to compensate for the loading effect. Fig. 4.13 shows the $|S_{11}|$ of the hairpin filter and the $|S_{11}|$ of the filter antenna integration, which is similar to the 3-pole bandpass filter function. The radiation pattern is shown in Fig. 4.14.

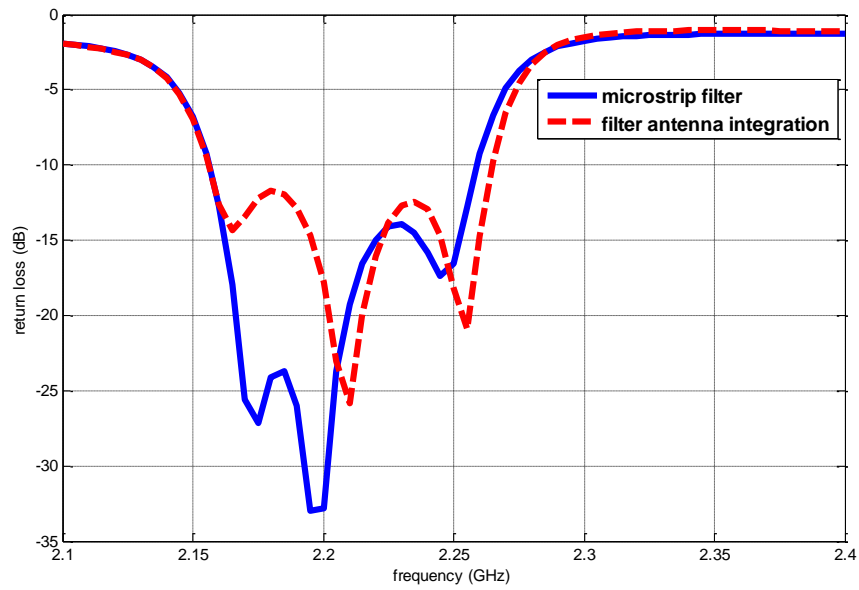


Fig. 4. 13. Reflection coefficients of the bandpass filter and the filter antenna integration.

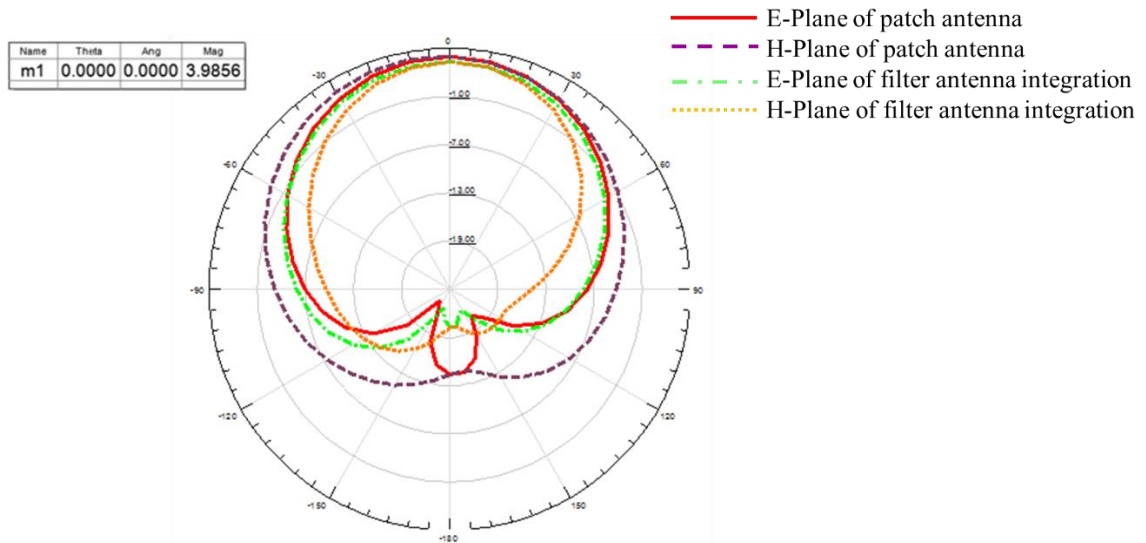


Fig. 4. 14. Simulated radiation pattern of the patch antenna and filter antenna integration.

4.5 Summary

Microstrip filter antenna integration is investigated in this chapter to improve the range of coupling value. It is shown that comparing to the reported values using proximity coupling [66], a much larger range of coupling coefficient can be readily achieved using the direct connection coupling method between the inset-fed patch antenna and the filter resonator. As a result, a wider design bandwidth can be realized.

CHAPTER 5

Conclusion and Future Work

The development of communication and radar systems raises the demand for circuits and systems with high performance. Filters and antennas are essential circuit elements. By removing transitions and connectors between filters and antennas in conventional systems, the integrated design of filters and antennas offers attractive features, such as compact size, low loss, and high efficiency. In this thesis, two types of filter and antenna integrations are investigated, namely the Substrate Integrated Waveguide (SIW) filter and dielectric resonator antenna (DRA) integration, and the microstrip filter and inset-fed microstrip patch antenna integration.

First of all, an SIW filter is designed to integrate with DRA. Using the DRA to replace the last resonator and the load of SIW filter, a compact integration functioning as a bandpass

filter and a radiator simultaneously is generated. The equivalent circuit models are adopted to analyze the coupling between filter and antenna. A design synthesis is presented, which can be applied to different filter and antenna integration designs in millimeter-wave and microwave frequency ranges. Design curves are presented, which can provide specific design values for required bandwidth. The designs are fabricated and measured. Shifts in frequency responses observed in the measurement results are analyzed to obtain a more accurate estimation of the substrate dielectric constant.

In addition, integrations of parasitic DRA and DRA array with SIW filter are also implemented. The results show that the design method can not only be used to single antenna element, but also be applied to antenna arrays.

Moreover, an inset-fed microstrip patch antenna is integrated with hairpin bandpass filter. The integration uses direct connection between the resonator and the microstrip antenna, and provides a large range of coupling coefficient. This method can be applied to wideband designs in microwave applications.

The following future work can be investigated:

- Another round of fabrication will be done with the more accurate estimate of the material property to further validate the designs developed in this thesis. In addition, an 8-element DRA array integrated with SIW filter will be built and tested.
- Due to the high operating frequency and filtering characteristics, the resonators of SIW filter are very sensitive to fabrication tolerances. Tuning structures consisting of tuning screws and/or slots on the SIW will be investigated and applied to the cavities to facilitate tuning of the circuits. As a result, improved performance can be achieved.

- The synthesis and tuning methods used in the thesis can be applied to filters and antennas realized in other technologies and for other applications.

BIBLIOGRAPHY

- [1] D. Deslandes and K. Wu, "Single-substrate integration technique of planar circuits and waveguide filters," *IEEE Trans. Microw. Theory Techn.*, vol. 51, no. 2, pp. 593–596, Feb. 2003.
- [2] D. Deslandes and K. Wu, "Integrated microstrip and rectangular waveguide in planar form," *IEEE Microw. Wireless Compon. Lett.*, vol. 11, no. 2, pp. 68–70, Feb. 2001.
- [3] F. Xu, and K. Wu, "Guided-wave and leakage characteristics of Substrate Integrated Waveguide", *IEEE Trans. Microwave Theory Tech.*, vol. 53, No. 1, pp. 66-73, January 2005.
- [4] J. H. Lee, N. Kidera, S. Pinel, J. Laskar, M. M. Tentzeris, "V-band integrated filter and antenna for LTCC front-end modules," in *Proc. IEEE MTT-S Int. Microw. Symp.*, Jun. 2006, pp. 978–981.
- [5] H. An. Nauwelaers, A. Van De Capalle, "A new approach of broadband microstrip antenna design," *IEEE AP-S Dig.*, Jun. 1992, pp. 475-478.
- [6] F. Queudet, I. Pele, B. Froppier, Y. Mahe, and S. Toutain, "Integration of pass-band filters in patch antennas," in *Proc. 32th Eur. Microw. Conf.*, 2002, pp. 685–688.
- [7] N. Yang, C. Caloz, and K. Wu, "Co-designed CPS UWB filter-antenna system," in *Proc. IEEE AP-S Int. Symp.*, Jun. 2007, pp. 1433–1436.
- [8] Abbaspour-Tamijani, J. Rizk, and G. Rebeiz, "Integration of filters and microstrip antennas," in *Proc. IEEE AP-S Int. Symp.*, Jun. 2002, pp. 874–877.

- [9] J.H.Zuo and X.W.Chen et al, “An Integrated Approach to RF AntennaFilter Co-Design,” *IEEE Antennas and Wireless Propag.*, vol. 8, pp. 141–144. Jan.2009.
- [10] O. A. Nova, J. C. Bohóquez, N. M. Pena, G. E. Bridges, L. Shafai, and C. Shafai, “Filter-antenna module using substrate-integrated waveguide cavities,” *IEEE Antennas Wireless Propag. Lett.*, vol. 10, pp. 59–62, Jan. 2011.
- [11] Z. Zakaria, W. Y. Sam, M. Z. A. Abd Aziz, A. Awang Md Isa, and F. Mohd Johar, “Design of Integrated Rectangular SIW Filter and Microstrip Patch Antenna”, *IEEE Asia-Pacific Conference on Appl. Electromagn. (APACE)*, pp. 137-141, Dec. 2012.
- [12] J.-S. Hong, *Microstrip Filter for RF/Microwave Applications*, 2nd ed. Hoboken, NJ, USA: Wiley, 2011.
- [13] Y. Quéré, C. Quendo, W. El Hajj, and C. Person, “A global synthesis tool and procedure for filter-antenna co-design,” in *Proc. 15th Int. Symp. Antenna Technol. Appl. Electromagn.*, Jun. 2012, pp. 1–4.
- [14] H.M. Hizan, I.C. Hunter, and A.I. Abunjaileh, “Integrated SIW Filter and Microstrip Antenna”, in *40th European Microwave Conf. Proc.*, pp. 184– 187, 2010.
- [15] C.-K. Lin and S.-J. Chung, “A filtering microstrip antenna array,” *IEEE Trans. Microw. Theory Techn.*, vol. 59, no. 11, pp. 2856–2863, Nov. 2011.
- [16] Y. Yusuf and X. Gong, “Co-designed substrate-integrated waveguide filters with patch antennas,” *IET Antennas, Propag.*, vol. 7, no. 7, pp. 493–501, Apr. 2013
- [17] R. J. Cameron, C. M. Kudsia, and R. R. Mansour, *Microwave Filters for Communication Systems: Fundamentals, Design, and Applications*. Hoboken, NJ, USA: Wiley, 2007.
- [18] D. M. Pozar, *Microwave Engineering*, 4th ed. Hoboken, NJ, USA: Wiley, 2011.

- [19] Y. Yusuf and X. Gong, "Compact low-loss integration of high-Q 3-D filters with highly efficient antennas," *IEEE Trans. Microw. Theory Techn.*, vol. 59, no. 4, pp. 857–865, Jan. 2011.
- [20] C.-K. Lin and S.-J. Chung, "A compact edge-fed filtering microstrip antenna with 0.2 dB equal-ripple response," in *Proc. 39th Eur. Microw. Conf.*, Rome, Italy, Sep. 29–Oct. 1, 2009, pp. 378–380.
- [21] H. M. Hizan, I. C. Hunter, and A. I. Abunjaileh, "Integrated dual-band radiating bandpass filter using dual-mode circular cavities," *IEEE Microw. Wireless Compon. Lett.*, vol. 21, no. 5, pp. 246–248, May 2011.
- [22] C. K. Lin and S. J. Chung, "A compact filtering microstrip antenna with quasi-elliptic broadside antenna gain response," *IEEE Antennas Wireless Propag. Lett.*, vol. 10, pp. 381–384, 2011.
- [23] Z. Zakaria, W.Y. Sam, M.Z.A. Abd Aziz, and M.M. Ismail, "The Integration Of Rectangular SIW Filter and Microstrip Patch Antenna Based On Cascaded Approach," *Procedia Engineering, Elsevier*, vol. 53, no. 1, pp. 347-353, 2013.
- [24] G. Mansour, M. J. Lancaster, P. S. Hall, P. Gardner and E. Nugoolcharoenlap, "Design of Filtering Microstrip Antenna Using Filter Synthesis Approach," *Progress in Electromagnetics Research (PIER)*, vol. 145, 2014, pp. 59-67.
- [25] I. Abunjaileh, I. C. Hunter, and A. H. Kemp, "Application of dualmode filter techniques to the broadband matching of microstrip patch antennas," *IET Microw., Antennas. Propag.*, vol. 1, pp. 273–276, 2007.

- [26] H. Chu, C. Jin, J.-X. Chen, and Y.-X. Guo, "A 3-D millimeter-wave filtering antenna with high selectivity and low cross-polarization," *IEEE Trans. Antennas Propag.*, vol. 63, no. 5, pp. 2375–2380, Mar. 2015.
- [27] B. Ding, X.-B. Wei, C. Wang, M.-X. Zhang, Z.-T. He, and Y. Shi, "A compact printed filtering antenna with flat gain using annular slot and UIR," in *Proc. 15th Int. Conf. Electron. Packag. Technol.*, Aug. 2014, pp. 1252–1255
- [28] H. Dashti, M. Shahabadi, M.H. Neshati, "SIW cavity-backed slot antennas with improved gain," *21st Iranian Conference on Electrical Engineering (ICEE)*, 2013 May 2011, pp.1-4
- [29] R. K. Mongia and A. Ittipiboon, "Theoretical and experimental investigations on rectangular dielectric resonator antennas," *IEEE Trans. Antennas Propag.*, vol. 45, no. 9, pp. 1348–1356, Sep. 1997.
- [30] R. K. Mongia, A. Ittipiboon, and M. Cuhaci, "Measurements of radiation efficiency of dielectric resonator antennas," *IEEE Microw. Guided Wave Lett.*, vol. 4, no. 3, pp. 80–82, Mar. 1994.
- [31] B. Li and K. W. Leung, "On the differentially fed rectangular dielectric resonator antenna," *IEEE Trans. Antennas Propag.*, vol. 56, no. 2, pp. 353–359, 2008.
- [32] Y. F. Wang, T. A. Denidni, Q.-S. Zeng, and G. Wei, "Design of high gain, broadband cylindrical dielectric resonator antenna," *Electron. Lett.*, vol. 49, no. 24, pp. 1506–1507, Nov. 2013.
- [33] K. W. Leung, K. M. Luk, K. Y. A. Lai, and D. Lin, "Theory and experiment of a coaxial probe fed hemispherical dielectric resonator antenna," *IEEE Trans. Antennas Propag.*, vol. 41, no. 10, pp. 1390–1398, Oct. 1993

- [34] G. P. Junker, A. A. Kishk, and A. W. Glisson, "Input impedance of dielectric resonator antennas excited by a coaxial probe," *IEEE Trans. Antennas Propag.*, vol. 42, no. 7, pp. 960–966, Jul. 1994
- [35] M. Abedian, S. K. A. Rahim, S. Danesh, C. Fumeaux, and T. A. Rahman, "Compact Wideband Probe-Fed Dielectric Resonator Antenna for X-Band Applications," *10th. Eurp. Conf. on Antennas Propag.*, 10-15, April 2016
- [36] Rashidian, M. Tayfeh Aligodarz, L. Shafai, and D. M. Klymyshyn, "On the matching of microstrip-fed dielectric resonator antennas," *IEEE Trans. Antennas Propag.*, vol. 61, no. 10, pp. 5291–5296, Oct. 2013.
- [37] R. A. Kranenburg, S. A. Long, and J. T. Williams, "Coplanar waveguide excitation of dielectric resonator antennas," *IEEE Trans. Antennas Propag.*, vol. 39, pp. 119–122, 1991.
- [38] K. W. Leung and K. K. So, "Waveguide-excited dielectric resonator antenna," in *Proc. IEEE Antennas and Propagation Society Int. Symp.*, 2001, vol. 2, pp. 132–135.
- [39] F. Shigeki, "Waveguide line," (*in Japanese*) *Japan Patent* 06-053 711, Feb. 25, 1994.
- [40] Hirokawa and M. Ando, "Single-layer feed waveguide consisting of posts for plane TEM wave excitation in parallel plates", *IEEE Trans. Microw. Theory Tech.*, vol. 46, no. 5, pp. 625-630, 1998.
- [41] Feb. 25, 1994 Y. Cassivi , L. Perregrini , P. Arcioni , M. Bressan , K. Wu and G. Conciauro, "Dispersion characteristics of substrate integrated rectangular waveguide", *IEEE Microw. Wireless Compon. Lett.*, vol. 12, no. 9, pp. 333-335, 2002.

- [42] L. Yan , W. Hong , K. Wu and T. J. Cui, "Investigations on the propagation characteristics of the substrate integrated waveguide based on the method of lines", *Proc. Inst. Elect. Eng.—Microw. Antennas Propag.*, vol. 152, pp. 35-42, 2005.
- [43] D. Pissort and F. Olyslager, "Study of eigenmodes in periodic waveguides using the Lorentz reciprocity theorem", *IEEE Trans. Microw. Theory Tech.*, vol. 52, no. 2, pp. 542-553, 2004.
- [44] F. Xu and K. Wu, "Numerical multimode calibration technique for extraction of complex propagation constants of substrate integrated waveguide", *IEEE MTT-S Int. Microw. Symp. Dig.*, pp. 1229-1232, 2004.
- [45] Zeid and H. Baudrand, "Electromagnetic scattering by metallic holes and its applications in microwave circuit design", *IEEE Trans. Microw. Theory Tech.*, vol. 50, no. 4, pp. 1198-1206, 2002
- [46] D. Deslandes and K. Wu, "Accurate modeling, wave mechanism, and design consideration of a substrate integrated waveguide," *IEEE Trans. Microw. Theory Tech.*, vol. 54, no. 6, pp. 2516–2526, Jun. 2006
- [47] D. Deslandes and K. Wu, "Design consideration and performance analysis of substrate integrated waveguide components", *Proc. 32th Eur. Microw. Conf.*, vol. 2, pp. 881-884, 2002.
- [48] X. Luan and K. Tan, "A Novel Ridge Substrate Integrated Waveguide Antenna for WLAN Application," *Antenna Techn. (iWAT)*., March 2011, pp. 302-305.
- [49] T. Y. Huang, T. M. Shen, H.-Y. Chien, and R. B. Wu, "Design of miniaturized vertically stacked SIW filters in LTCC," in *Eur. Microw. Conf.*, Sep. 2009, pp. 413–416.

- [50] S. Sirci, F. Gentili, J. Martínez, V. Boria, and R. Sorrentino, “Quasi-Elliptic Filter Based on SIW Compline Resonators Using a Coplanar Line Cross-Coupling,” *IEEE MTT-S Int. Microwave Symp.*, pp.1-4, May. 2015.
- [51] R. S. Chen, S.-W. Wong, L. Zhu, and Q.-X. Chu, “Wideband bandpass filter using U-slotted substrate integrated waveguide (SIW) cavities,” *IEEE Microw. Wireless Compon. Lett.*, vol. 25, no. 1, pp. 1–3, Jan. 2015.
- [52] Z.-C. Hao, W. Hong, J.-X. Chen, X.-P. Chen, and K. Wu, “Compact super-wide bandpass substrate integrated waveguide (SIW) filters,” *IEEE Trans. Microw. Theory Tech.*, vol. 53, no. 9, pp. 2968–2977, Sep. 2005.
- [53] D. Deslandes and K. Wu, “Single-substrate integration technique for planar circuits and waveguide filters,” *IEEE Trans. Microw. Theory Tech.*, vol. 51, no. 2, pp. 593–596, Feb. 2003.
- [54] X.-P. Chen and K. Wu, “Substrate integrated waveguide cross-coupled filter with negative coupling structure,” *IEEE Trans. Microw. Theory Tech.*, vol. 56, no. 1, pp. 142–149, Jan. 2008.
- [55] M. Abdolhamidi and M. Shahabadi, “X-band substrate integrated waveguide amplifier,” *IEEE Microw. Wireless Comp. Lett.*, vol. 18, pp. 815–817, 2008.
- [56] T. Y. Yang, W. Hong, and Y. Zhang, “Wideband millimeter-wave substrate integrated waveguide cavity-backed rectangular patch antenna,” *IEEE Antennas Wireless Propag. Lett.*, vol. 13, pp. 205–208, Jan. 2014.
- [57] W. M. A. Wahab, D. Busuioc, and S. Safavi-Naeini, “Low cost planar waveguide technology-based dielectric resonator antenna (DRA) for millimeter-wave

- applications: Analysis, design, fabrication,” *IEEE Trans. Antennas Propag.*, vol. 58, no. 8, pp. 2499–2507, Aug. 2010.
- [58] Z. C. Hao, W. Hong, A. Chen, J. Chen, and K. Wu, “SIW fed dielectric resonator antennas (SIW-DRA) ,” *IEEE MTT-S Int. Microwave Symp.*, pp. 202–205, Jun. 11–16, 2006.
- [59] Ke Gong; Xue Hui Hu, “Low-profile substrate integrated dielectric resonator antenna implemented with PCB process,” *IEEE Antennas Wireless Propaga. Lett.*, vol.13, no., pp.1023-1026, 2014.
- [60] L. Young, “Direct-coupled cavity filters for wide and narrow bandwidths,” *IEEE Trans. Microw. Theory Tech.*, vol. MTT-11, no. 3, pp. 162–178, May 1963.
- [61] Y. Yusuf and X. Gong, “Compact low-loss integration of high-Q 3-D filters and highly efficient slot antennas,” *IEEE Trans Microw. Theory Tech.*, vol. 59, no. 4, pp. 857–865, Apr. 2011.
- [62] S. Koziel, Q. S. Cheng, and J. W. Bandler, “Space mapping,” *IEEE Microw. Mag.*, vol. 9, no. 6, pp. 105–122, Dec. 2008.
- [63] T. Seki, K. Nishikawa, I. Toyoda, and S. Kubota, “Microstrip array antenna with parasitic elements alternately arranged over two layers of LTCC substrate for millimeter wave applications,” in *Proc. IEEE Radio and Wireless Symp.*, Long Beach, CA, Jan. 9–11, 2007, pp. 149–152.
- [64] K.F. Lee, R.Q. Lee, and T. Talty, "Microstrip Subarray with Coplanar and Stacked Parasitic Elements", *Electronics Lett.*, Vol. 26, pp. 668- 669, 1990.

- [65] M. Ranjbar-Nikkhah, J. Rashed-Mohassel, and A. A. Kishk, "Compact low-cost phased array of dielectric resonator antenna using parasitic elements and capacitor loading," *IEEE Trans. Antennas Propag.*, vol. 61, no. 4, pp. 2318–2321, Apr. 2013.
- [66] G. Mansour, M. J. Lancaster, P. S. Hall, P. Gardner, and E. Nugoolcharoenlap, "Design of filtering microstrip antenna using filter synthesis approach," *Progress in Electromagnetics Research (PIER)*, vol. 145, 2014, pp. 59-67.
- [67] S. Weigand, G. H. Huff, K. H. Pan, and J. T. Bernhard, "Analysis and design of broadband single-layer rectangular U-slot microstrip patch antennas," *IEEE Trans. Antennas Propag.*, vol. 51, no. 3, pp. 457–468, Mar. 2003.
- [68] M. R. Ahsan, M. T. Islam, M. Habib Ullah, W. N. L. Mahadi, and T. A. Latef, "Compact double-P slotted inset-fed microstrip patch antenna on high dielectric substrate," *The Scientific World Journal*, 2014.
- [69] V. V. Thakare and P. K. Singhal, "Bandwidth analysis by introducing slots in microstrip antenna design using ANN," *Prog. Electromagn. Res. M*, vol. 9, pp. 107-122, 2009.
- [70] Z. Zakaria, W.Y. Sam, M. Z. A. Abd Aziz, and M. A. Meor Said, "Rectangular Microstrip Patch Antenna Based on Resonant Circuit Approach," *IEEE Symposium on Wireless Technology and Applications (ISWTA)*, pp.233-236, 2012.
- [71] K. F. Tong, K. M. Luk, K. F. Lee, and R. Q. Lee, "A broad-band U-slot rectangular patch antenna on a microwave substrate," *IEEE Trans. On Ant. Propag.*, vol. AP-48, no. 6, pp. 954-960, June 2000.

- [72] M. A. Matin, B. S. Sharif, C. C. Tsimenidis, "Probe Fed Stacked Patch Antenna for Wideband Applications," *IEEE Trans. Antennas Propag.*, vol. 55, no. 8, pp. 2385-2388, Aug. 2007.
- [73] P. Sharma and S. Gupta, "Bandwidth and gain enhancement in microstrip antenna array for 8GHz frequency applications," in *Engineering and Systems (SCES), 2014 Students Conference on*, 2014, pp. 1-6.
- [74] D. Sun and L. You, "A broadband impedance matching method for proximity-coupled microstrip antenna," *IEEE Trans. Antennas Propag.*, vol. 58, no. 4, pp. 1392-1397, Apr. 2010.
- [75] K.R. Carver, and S.W. Mink, "Microstrip antenna technology," *IEEE Trans. Antennas Propag.*, vol. AP-29, pp. 2-24, Jan. 1981.
- [76] J. R. James, P. S. Hall, and C. Wood, *Microstrip Antenna: Theory and Design*. Stevenage, UK: Peter Peregrinus, 1981.
- [77] Prasanna L. Zade1, Dr. N. K. Choudhary and M. S. Narlawar "EM optimization of an inset fed rectangular microstrip antenna as a function of inset depth and width for wireless communication", *International Conference on New Trends in Information and Service Science*, pp.100-104, 2009.